

Wall slip and flow of concentrated hard-sphere colloidal suspensions

P. Ballesta,^{1,2} G. Petekidis,^{2,3} L. Isa,^{1,4} W. C. K. Poon,¹ and R. Besseling¹

¹*Scottish Universities Physics Alliance (SUPA) and School of Physics and Astronomy, The University of Edinburgh, Kings Buildings, Mayfield Road, Edinburgh EH9 3JZ, United Kingdom.*

²*IESL-FORTH, Heraklion 71110, Crete, Greece.*

³*Department of Materials Science and Technology, University of Crete, Heraklion 71110, Crete, Greece.*

⁴*ETH Zurich, Laboratory for Surface Science and Technology, Wolfgang-Pauli-Strasse 10, Zürich, Switzerland.*

(Dated: 27 November 2024)

We present a comprehensive study of the slip and flow of concentrated colloidal suspensions using cone-plate rheometry and simultaneous confocal imaging. In the colloidal glass regime, for smooth, non-stick walls, the solid nature of the suspension causes a transition in the rheology from Herschel-Bulkley (HB) bulk flow behavior at large stress to a Bingham-like slip behavior at low stress, which is suppressed for sufficient colloid-wall attraction or colloid-scale wall roughness. Visualization shows how the slip-shear transition depends on gap size and the boundary conditions at both walls and that partial slip persists well above the yield stress. A phenomenological model, incorporating the Bingham slip law and HB bulk flow, fully accounts for the behavior. Microscopically, the Bingham law is related to a thin (sub-colloidal) lubrication layer at the wall, giving rise to a characteristic dependence of slip parameters on particle size and concentration. We relate this to the suspension's osmotic pressure and yield stress and also analyze the influence of van der Waals interaction. For the largest concentrations, we observe non-uniform flow around the yield stress, in line with recent work on bulk shear-banding of concentrated pastes. We also describe residual slip in concentrated liquid suspensions, where the vanishing yield stress causes coexistence of (weak) slip and bulk shear flow for all measured rates.

PACS numbers: 83.50.Ax, 83.60.-a, 83.80.Hj, 83.85.Ei

I. INTRODUCTION

Wall slip is a widespread phenomenon in the flow of various liquids. In Newtonian liquids, interest in slip has revived due to its relevance for flow in nano-porous media, microfluidic devices and along superhydrophobic surfaces [Barrat and Bocquet (1999); Zhu and Granick (2001); Bocquet and Barrat (2007); Neto *et al.* (2004)]. The so-called slip-length l_s , the distance to the wall at which the velocity profile extrapolates to zero, can reach many molecular diameters, depending on wettability, and strongly affects flow when it is comparable to the system dimensions. Polymer slip has also received considerable attention, e.g. [Hatzikiriakos and Dealy (1991, 1992); Brochardt and de Gennes (1992); Westover (1966); Léger *et al.* (1997); Mhetar and Archer (1998)]. Here changes in the chain relaxation dynamics near the wall govern slip: typically a transition from weak slip at small flow rate to strong slip (l_s exceeding hundreds of micrometers [Mhetar and Archer (1998)]) for large flow rate is seen, driven by chain disentanglement near the wall. In surfactant solutions, recent work [Salmon *et al.* (2003); Bécu *et al.* (2006); Manneville *et al.* (2004); Lettinga and Manneville (2009); Bécu *et al.* (2007)] has shown more complex behavior, where slip and wall interactions are coupled to the shear-banding in these systems.

The most prominent examples of slip in industrial and daily applications occur in flow of complex, multi-phase fluids [Yoshimura and Prud'homme (1988); Barnes (1995); Larson (1999)]. Meaningful characterization of the bulk flow properties of these systems requires proper insight into boundary effects [Buscall (2010)]. Over the last decades, many studies of slip in these systems have appeared, e.g. in particulate (colloidal) suspensions [Yilmazer and Kalyon (1989); Aral and Kalyon (1994); Hartman Kok *et al.* (2004); Kalyon (2005); Jana *et al.* (1995); Cohen *et al.* (2006); Isa *et al.* (2007); Soltani and Yilmazer (2008); Persello *et al.* (1994)], colloidal gels [Buscall *et al.* (1993); Russel and Grant (2000); Walls *et al.* (2003); Varadan and Solomon (2003); Gibaud *et al.* (2008); Wassenius and Callaghan (2005)] and emulsions and foams [Bertola *et al.* (2003); Princen (1985); Meeker *et al.* (2004a,b); Salmon *et al.* (2003); Denkov *et al.* (2005); Katgert *et al.* (2008)]. Despite this large body of work, it is challenging to gain microscopic insight into the nature of slip and understand its dependence on material composition, wall properties, and flow rate. Broadly speaking, slip results from depletion of the dispersed phase near a smooth wall, giving a low viscosity, high shear boundary layer which reduces

the *apparent* bulk viscosity ¹. However, both the structure and the origin of this “layer” vary greatly between different systems and the interplay with (non)linear bulk rheology can give rise to slip being pronounced either at large or small flow rate.

Slip at low stress or applied shear rate can occur in dispersions where caging, aggregation or ‘jamming’ leads to a solid-like microstructure and mechanical behavior. The system then exhibits a yield stress, σ_y , below which the micro-structure remains intact but, depending on wall interactions and roughness, *apparent* flow of the material can still be measured. This was recently studied for concentrated emulsions and other soft particle pastes [Meeker *et al.* (2004a); Seth *et al.* (2008)] in presence of smooth walls. There, elasto-hydrodynamic lubrication, associated with the particles’ deformability, causes a lubrication layer between the compressed packing and the wall with velocity dependent thickness. This gives a nonlinear relation between the slip stress σ and the slip velocity v_s , but this mechanism only occurs for very weakly or non-repulsive particle-wall interactions [Meeker *et al.* (2004b); Seth *et al.* (2008)]. Note that nonlinear lubrication is of strong interest to applications of many other soft solids, e.g. hydrogels, where combined wall-network repulsion and adsorption determines the friction properties [Gong and Osada (2010)].

For suspensions of ‘hard’ particles, most studies of slip have been performed for *non-Brownian* systems, i.e. at large Péclet number $Pe = \dot{\gamma}\tau_B \gg 100$, where $\dot{\gamma}$ is the true bulk flow rate and τ_B the Brownian relaxation time. There, slip occurs both in solid- [Yilmazer and Kalyon (1989); Kalyon (2005)] and liquid-like [Jana *et al.* (1995)] suspensions (albeit without consensus on the quantitative behavior), but little attention has been given to the effect of Brownian motion on slip in colloidal systems. Hartman Kok *et al.* (2004) found that Brownian motion prevents depletion at low shear rates in dilute colloids, so that slip becomes apparent only for $Pe \gtrsim 10$. However, for more concentrated colloids, ‘crowding’ competes with Brownian relaxation. This causes structural arrest, a glass transition [Pusey and van Meegen (1986); van Meegen *et al.* (1998)], which for hard-sphere (HS) colloids occurs at a volume fraction of $\phi_g \simeq 0.58$. The associated change from liquid to solid-like rheology [Petekidis *et al.* (2004)] can significantly affect the slip response.

The slip and flow behavior in these concentrated HS colloidal suspensions is the subject of this paper. In [Ballesta *et al.* (2008)] we have given a short account of some of the

¹ We refer here to ‘intrinsic’ depletion under uniform stress, as opposed to depletion of dispersed phase due to shear migration as may arise under non-uniform stress.

results, here we present a more extensive study of the behavior. Using rheo-microscopy [Besseling *et al.* (2009)], we show that for $\phi > \phi_g$, slip becomes dominant in the rheology for smooth, non-stick walls. We address the dependence of slip on colloid-wall (van der Waals) interactions and concentration and quantitatively describe the transition from slip to yielding for different combinations of confining walls via a phenomenological model. Below the yield stress, slip causes full plug flow, qualitatively similar to jammed emulsions and microgels [Meeker *et al.* (2004a); Seth *et al.* (2008)], but quantitatively different; above a threshold stress, the slip stress increases linearly with the slip velocity (Bingham slip response) due to a sub-colloidal solvent layer with velocity-independent thickness. The concentration dependence of the Bingham slip parameters shows a direct relation to the osmotic pressure and yield stress of the suspensions, which can be understood on a semi-quantitative basis but still lacks a full theoretical description. We further show that deep in the glass regime, shear localization effects [Besseling *et al.* (2010)] accompany the slip-shear transition and discuss residual slip in concentrated liquid suspensions ($\phi < \phi_g$), a feature not uncovered previously [Ballesta *et al.* (2008)] due to its limited effect on the bulk rheology.

The paper is structured as follows. After a description of the measurement setup and suspensions in Sec. II, we present rheology and local velocimetry results for various hard sphere suspensions, colloid-wall interactions and confining walls conditions in Sec. III. In Sec. IV, we describe the phenomenological model for slip and yielding, generalizing the results in [Ballesta *et al.* (2008)] to account for geometries with various confining walls, and in Sec. V we compare the predictions with the experimental results. The physical origin of the Bingham slip parameters is analyzed in Sec. VI, along with the effect of van der Waals interactions. Sect. VII and VIII deal with shear localization for $\phi > \phi_g$ and residual slip in liquid suspensions for $\phi < \phi_g$, respectively, and we conclude in Sect. IX.

II. SAMPLES AND METHODS

A. Colloidal suspensions

We used polymethylmethacrylate (PMMA) colloids of various sizes (radii $a = 138$ nm, 150 nm, 302 nm and a fluorescent batch with $a = 652$ nm, measured by light scattering, polydispersity $\sim 15\%$), sterically stabilized with a poly-12-hydroxystearic acid (PHSA) layer

[Barret (1974)] and dispersed in a refractive index (RI) matching solvent mixture of decalin and tetralin (viscosity $\eta_s = 2.2$ mPas). A few measurements were also conducted using pure decalin as solvent. Non-fluorescent (RI-matched) samples were seeded with $\sim 0.5\%$ of the fluorescent particles (labeled with nitrobenzoxadiazole, NBD), which served as tracers during confocal imaging (Fig. 1(b)). In these solvents the colloids interact almost like perfect HSs [Bryant *et al.* (2002)]. In the decalin-tetralin mixture the refractive index of the colloids is $\sim 1.50 - 1.51$, somewhat larger than the bulk PMMA value (1.49), due to solvent absorption of the colloids and slight swelling, estimated to be $\sim 10\%$.

Batches of different volume fractions ϕ were prepared by diluting samples centrifuged to a random close packed sediment, with volume fraction $\phi_{sed} = \phi_{rcp}$. One traditional method to determine ϕ for HS suspensions employs the crystal-fluid coexistence boundaries [Segré *et al.* (1995); Pusey and van Megen (1986)]. Because of polydispersity our suspensions do not crystallize, and ϕ has to be determined differently [Poon *et al.* (2011)]. We have chosen the following method. We first measure the mass density of the solvent ρ_s (densitometer: Anton Paar DMA 4500). We then measure the density ρ_{rcp} of the close packed sediment after centrifugation by taking a small sample, diluting it by a factor $f = 10$ by weight in solvent and measuring the density ρ^* of this diluted suspension. The density of the sediment is then deduced from $\rho_{rcp} = \rho^* \rho_s / [(1 + f)\rho_s - f\rho^*]$. Samples at a given $\phi/\phi_{rcp} < 1$ for the main experiments are then prepared by adding a solvent mass M_s to the known weight M_t of the stock sediment (giving $\phi/\phi_{rcp} = [1 + \frac{M_s \rho_{rcp}}{M_t \rho_s}]^{-1}$) and homogenizing the sample rigorously. The densitometry results are given in table I; ρ_s slightly increases with increasing particle size, probably due to a slight increase in RI for larger particles and thus a slight change in the RI-matching composition of the solvent mixture. We emphasize that, without knowledge of the colloid mass density ρ_c , this method does not provide ϕ_{rcp} but only ϕ/ϕ_{rcp} . When mentioning absolute volume fractions, we have assumed $\phi_{rcp} = 0.67$, as found in simulations of spheres with a polydispersity of $\sim 15\%$ [Schaertl and Sillescu (1994)] (monodisperse spheres give $\phi_{rcp} = 0.64$). The value of $\phi_{rcp} = 0.67$ may be used to extract the colloid density via $\phi_{rcp} = (\rho_{rcp} - \rho_s)/(\rho_c - \rho_s)$. The resulting densities $\rho_c \sim 1.12 - 1.13$ g/ml are reduced compared to the bulk PMMA value of ~ 1.2 g/ml, but reasonable match what is expected from the above mentioned $\sim 10\%$ swelling of the particles ². We note that the effect of polydispersity and compaction rate on the value of ϕ_{rcp} is still

² We do not separately take into account the reduction of ρ_c arising from the PHS-layer. The density of

sample name	asm340	asm247	asm209	asm195
a (nm)	138	150	300	652
ρ_s (g.ml ⁻¹)	0.9153	0.915	0.92023	0.92543
ρ_{RCP} (g.ml ⁻¹)	1.0596	1.0594	1.07	1.0644

TABLE I. Particle size a , density of the index-matched solvent ρ_s and density of the random close packed sediment ρ_{RCP} for the different samples.

under study [Hermes and Dijkstra (2010)] and not without controversy, see also [Poon *et al.* (2011)]. Yet, in relative terms, our approach is quite accurate, the main uncertainty being a variation $\delta\phi_{r_{cp}}/\phi_{r_{cp}} \simeq 0.005$ found between different centrifugation runs via drying and weighting. The value of this uncertainty is close to the maximum variation in the ‘jamming’ fraction for our polydispersity, as found in simulations of HSs for different compression rates [Hermes and Dijkstra (2010)], but our $\delta\phi_{r_{cp}}$ (in two tests we performed, using a single batch) was obtained under similar centrifugation conditions. Moreover, the sedimentation Peclet number $Pe_s = 4\pi a^4 \Delta\rho g_c / 3k_B T$ (with $\Delta\rho = \rho_c - \rho_s$ and g_c the acceleration), lies in the range $Pe_s \sim 0.005 - 1$ from the smallest to the largest particles. Thus, ‘jamming’ effects (which may cause $\phi_{sed} < \phi_{r_{cp}}$) are strongly limited, except possibly for the $a = 652$ nm sample. Most important, for the analysis of the ϕ dependence of rheological and slip parameters (Sect. VI), we employ the directly measured *reduced* volume fraction $\phi/\phi_{r_{cp}}$, which suffers the least from possible ambiguities [Poon *et al.* (2011)].

B. Measurement system

We use a stress-controlled rheometer (AR2000, TA Instruments) with a cone-plate geometry (radius $r_c = 20$ mm, cone angle $\theta = 1^\circ$ unless mentioned otherwise) and a glass slide (radius 25 mm, thickness ~ 180 μm) as the bottom plate. A solvent trap saturates the atmosphere around the sample minimizing evaporation. We image the flow with a confocal scanner (VT-Eye, Visitech International) through the glass plate via a piezo-mounted objective (oil immersion, magnification $\geq 60\times$), and optics mounted on an adjustable arm

swollen colloids is then simply $\rho_c = (\rho_{PMMAS} s^{-3}) + [1 - s^{-3}]\rho_s$ with $s \simeq 1.1$ the swelling ratio. As the swelling is not exactly known, we have used bare particle radii, measured in decalin, throughout the paper.

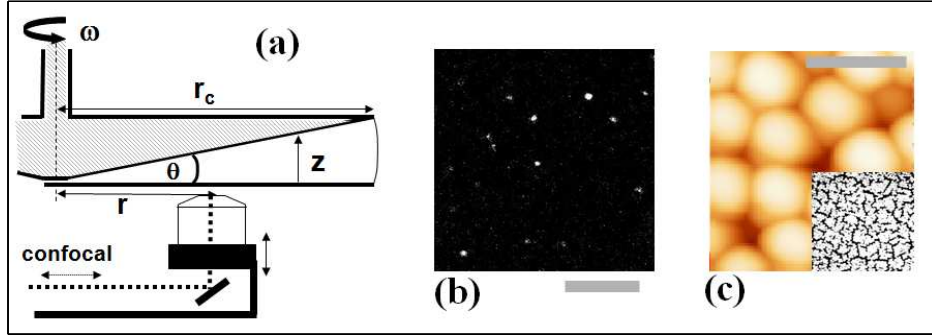


FIG. 1. (a) Cone-plate rheometer with transparent plate and optics connected via an adjustable arm to the confocal scanner. The cone angle θ and radius r_c are shown. (b) Confocal image of an RI-matched suspension with the $a = 652$ nm fluorescent tracers showing as bright spots. Scale bar: $10 \mu\text{m}$. (c) AFM image of the sintered layer of $a = 652$ nm colloids on the glass slide. The color scale marks height variations of ~ 500 nm. Scale bar: $2.5 \mu\text{m}$. Inset: confocal image of a coated slide on a larger scale, $50 \times 50 \mu\text{m}$.

[Besseling *et al.* (2009)]. We take 2D movies in the flow-vorticity (x - y) plane at a frame rate ≤ 90 Hz at various distances r from the cone center and at equally spaced depths $z \leq h$, with z the velocity-gradient direction and h the local gapsize (Fig. 1(a)), from which we extract, via image analysis [Besseling *et al.* (2009)], the velocity profiles $v(z)$ at different r . The typical error bar in the reduced velocity $v(z)/v(h)$ is $\lesssim 5\%$, achieved by imaging sufficiently large displacements, i.e. over timescales of at least a few times $1/\dot{\gamma}_a$ (see also [Besseling *et al.* (2010)]). The observation window is $\sim 50 \times 50 \mu\text{m}^2$, similar to the gap sizes where imaging is performed ($r = 2$ – 10 mm, $h = 35$ – $175 \mu\text{m}$). Over the observation window, the variation in h ($\delta h \simeq 0.9 \mu\text{m}$) is negligible, $\delta h/h \ll 1$, and the geometry locally mimics parallel plates separated by $h = r \tan(\theta)$. Experiments were performed at controlled applied shear rate $\dot{\gamma}_a$ (using the rheometer’s fast feedback), going from high to low rates, unless stated otherwise. Stress controlled measurements gave the same results; in particular, we do not find differences between ‘static’ (measured for increasing stress) and dynamic stress thresholds for flow or slip (the latter measured on reducing σ or $\dot{\gamma}_a$), except for possible initial hysteresis just after loading of very concentrated samples (Sect. VI).

C. Wall properties

We have used the following preparations of the surfaces of the cone-plate geometry: (i) To prevent slip, the cone, the glass slide or both can be made rough on a scale similar to or larger than the particle radius by spin-coating a $\phi \sim 0.3$ suspension of $a = 652$ nm radius particles and sintering the resulting dense disordered colloidal monolayer for one hour at $\sim 120^\circ$ C in a vacuum oven. This sintering causes adhesion of the colloids to the glass (or metal cone), probably accompanied by local redistribution of the PHS stabilizer at these temperatures. Nevertheless, the sintering leaves the corrugated nature of the disordered monolayer intact, giving a wall roughness ~ 500 nm, see Fig. 1(c) and the inset. The suppression of slip associated with this rough coating has been evidenced in [Besseling *et al.* (2009)] (Fig. 16 in that paper) and is also shown in Sect. VII. (ii) Use of the glass slides without coating gives a surface which is very smooth on the colloidal scale (local roughness < 1 nm measured by AFM). The slides were used either untreated or cleaned with ethanol, methanol or a Piranha solution (98% H_2SO_4 :30% H_2O_2 aqueous solution, ratio 7 : 3 by mass), but these cleaning methods did not give systematic differences in slip behavior. We also performed temperature-controlled rheological measurements (without imaging) using the smooth glass slides as bottom plate, achieved by anchoring the slides on the rheometer Peltier plate using thermal paste. The stainless steel surface of the cone (cleaned with acetone) is also smooth on the colloidal scale, but interacts differently with the colloids (Sect. VIB).

III. MAIN EXPERIMENTAL RESULTS

Rheological studies of concentrated HS suspensions have shown the emergence of a finite dynamic yield stress for $\phi \gtrsim 0.57 - 0.58$ [Petekidis *et al.* (2004); Pham *et al.* (2006)]. For $\phi < \phi_g$, the flow curve, i.e. a plot of the measured stress (σ_m) versus applied shear rate ($\dot{\gamma}_a$), exhibits Newtonian behavior at low $\dot{\gamma}_a$ followed by strong shear thinning at higher $\dot{\gamma}_a$, while for $\phi > \phi_g$ suspensions are glassy and have a yield stress σ_y below which no flow occurs. In this case the flow curves exhibit a Herschel-Bulkley behavior described by $\sigma_m = \sigma_y + \alpha \dot{\gamma}_a^n$. This behavior is geometry independent [Pham *et al.* (2008)], at least for $\phi \lesssim 0.6$, indicating that $\dot{\gamma}_a$ and the bulk flow rate of the material, $\dot{\gamma}$, are the same. For larger ϕ , different geometries may cause small differences for $\sigma \simeq \sigma_y$ due to shear-banding [Besseling *et al.*

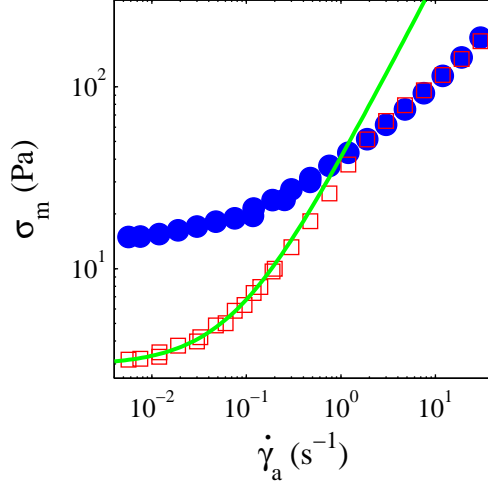


FIG. 2. Measured shear stress σ_m versus applied shear rate $\dot{\gamma}_a$ for $a = 300$ nm colloids at $\phi \sim 0.64$ in RI-matching solvent (\square) and decalin (\bullet), using a smooth glass slide and coated cone. Full line: fit of the low $\dot{\gamma}_a$ branch to Eq. (1), giving $\eta_{\text{eff}} = 38.3$ Pa·s, $\sigma_s = 2.94$ Pa. The data for decalin are multiplied by a factor 1.5 for comparison, the difference with the RI-matching solvent is due to slightly different ϕ .

(2010)], but the bulk $\sigma(\dot{\gamma})$ behavior is nevertheless consistent with a HB form.

We first illustrate how the rheology for $\phi > \phi_g$ is affected when the colloid-wall interaction is changed. Figure 2 shows the stress measured with the rheometer, σ_m , versus the *applied* shear rate $\dot{\gamma}_a$ for a suspension in pure decalin as well as in the RI-matching decalin-tetralin mixture, at similar volume fractions. For the RI-mismatched sample, the flow curve clearly shows a yield stress and an overall Herschel-Bulkley response. However, in the RI-matched sample, the flow curve at low $\dot{\gamma}_a$ exhibits a branch with Bingham-like behavior:

$$\sigma_m = \sigma_s + \eta_{\text{eff}} \dot{\gamma}_a. \quad (1)$$

Here σ_s is a threshold stress below which the (apparent) flow completely stops and η_{eff} is an effective viscosity characterizing the stress increase in this branch. For large $\dot{\gamma}_a$ the stress attains the same nonlinear behavior as the sample in decalin. As shown below, the small $\dot{\gamma}_a$ behavior marks full slip along the glass slide (due to the strongly suppressed colloid-wall vdW attraction) with a vanishing shear rate $\dot{\gamma}$ in the bulk of the sample.

We next discuss results for different combinations of smooth and colloid-coated surfaces. Figure 3 shows flow curves for RI-matched samples with both walls or one wall coated,

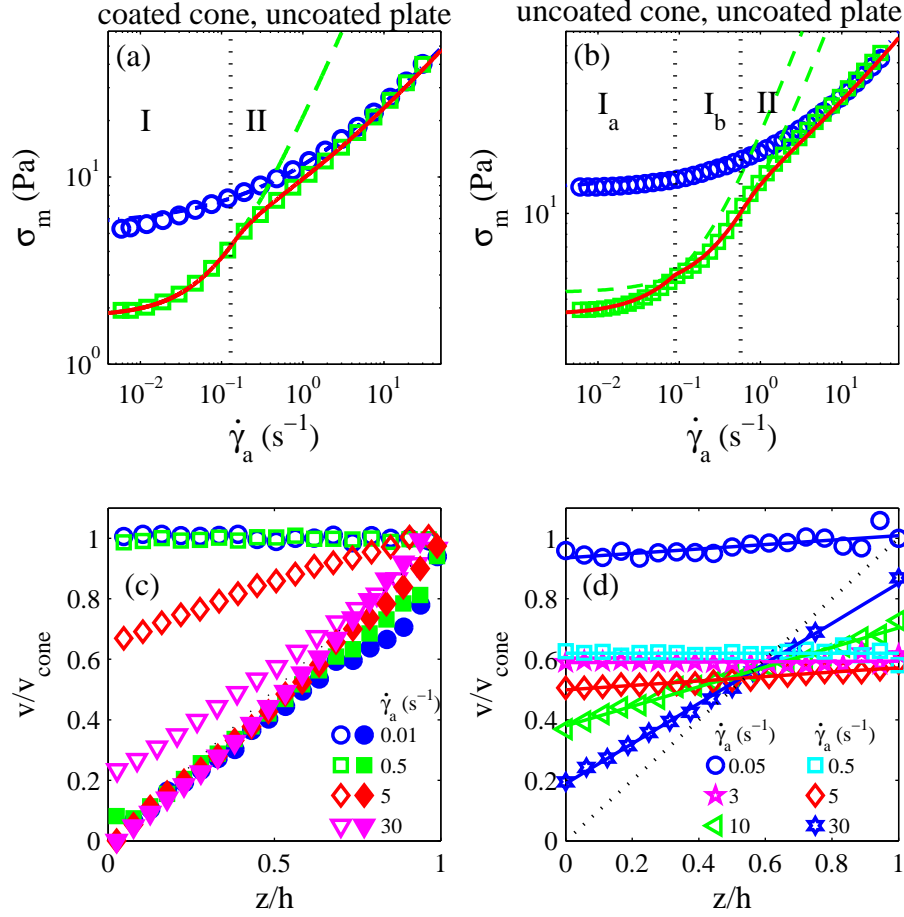


FIG. 3. (a,b) Measured stress versus $\dot{\gamma}_a$ for coated cone and plate (o) and with (a) uncoated plate (\square) and $\phi = 0.59$ and $a = 138$ nm, and (b) uncoated cone and uncoated plate (\square) with $\phi = 0.59$ and $a = 150$ nm. Regime I in (a) and I_a in (b) represent full slip along one boundary; regime I_b in (b) represents full slip along two boundaries; and regime II in (a),(b) mark slip plus bulk flow. In (a),(b) the dash-dot curves are Hershel-Bulkley fits with $n = 0.5$, Eq. (3), giving $\alpha = 6.1 \text{ Pa}\cdot\text{s}^{1/2}$, $\sigma_y = 5.5 \text{ Pa}$ in (a) and $\alpha = 8 \text{ Pa}\cdot\text{s}^{1/2}$, $\sigma_y = 14 \text{ Pa}$ in (b); dashed curves are fits to the Bingham form Eq. 1. In regime I in (a), where Eq. (10) applies, this gives $\beta = 8.2 \cdot 10^4 \text{ Pa s/m}$, $\sigma_s = 1.8 \text{ Pa}$. In regime I_a or I_b in (b), where Eq. (10) and Eq. (11) apply, the parameters are $\beta = 8.7 \cdot 10^4 \text{ Pa}\cdot\text{s}\cdot\text{m}^{-1}$, $\sigma_1 = 5.2 \text{ Pa}$, $\sigma_2 = 3.4 \text{ Pa}$; full lines in regime II are the global flow curves from Eq. A2 in Appendix A 1 using the above parameters. (c) Normalized velocity profiles $v(z)/v_{cone}$ for the suspension in (a) at $r = 3$ mm with coated surfaces (filled symbols) and at $r = 2.5$ mm with uncoated plate (open symbols) for various $\dot{\gamma}_a$. (d) $v(z)/v_{cone}$ for the data in (b) for uncoated cone and plate, at $r = 5.5$ mm and various $\dot{\gamma}_a$. Full lines: linear fits. Dotted lines: behavior without slip.

Fig. 3(a), and with two uncoated walls (smooth glass plate and stainless steel cone), Fig. 3(b). With both surfaces coated (Fig. 3(a), open circles), a Herschel-Bulkley behavior is recovered, confirming that coating prevents slip, as we also directly observed via microscopy [Besseling *et al.* (2007); Ballesta *et al.* (2008)]. If only one surface is coated (squares in Fig. 3(a)), we observe a similar slip response as described above: below a critical applied shear rate $\dot{\gamma}_{a,c}$ bulk shear vanishes in the entire gap (see below and the appendix) and we have a Bingham response; we define this as regime I. For $\dot{\gamma}_a > \dot{\gamma}_{a,c}$ the flow curve deviates from this Bingham regime and approaches the flow curve obtained with coated geometry, this regime is noted regime II. If both walls are uncoated, squares in Fig. 3(b), the flow curve exhibits two successive Bingham regimes at low shear rate: I_a marking slip at the plate, I_b marking slip at both surfaces (see Sec. IV); the second Bingham regime, I_b , has a higher slip stress and an effective viscosity η_{eff} half the value of that in regime I_a . Eventually, at high shear rate, the curve again tends toward the HB flow curve.

We now turn to the velocimetry results obtained by simultaneous confocal imaging of the flow, Fig. 3(c,d). In Fig. 3(c) the filled symbols show flow profiles with both walls coated. These profiles are nearly linear and $v(z)$ reaches zero at the glass plate and the applied velocity at the cone, showing that the coating provides a no-slip condition. The open symbols in Fig. 3(c),(d) show $v(z)$ for one uncoated surface (c) or two uncoated surfaces (d). In both cases $v(z)$ is essentially linear but exhibits slip at the non-coated walls. The profiles can be fitted by $v = v_s + \dot{\gamma}z$, with v_s the slip velocity at the plate and $\dot{\gamma}$ the bulk shear rate. At the smallest $\dot{\gamma}_a$, $\dot{\gamma}$ is zero; the suspension sticks to the coated cone and rotates as a solid body, slipping over the smooth glass. This causes the apparent flow below the yield stress in regime I in Fig. 3(a) or I_a in (b). Figure 3(c) shows that plug flow can persist in regime II for $r = 2.5$ mm and $\dot{\gamma}_a = 0.5$ s⁻¹, as explained later. With two uncoated surfaces, Fig. 3(d), the velocity profiles for intermediate $\dot{\gamma}_a$ show slip at both walls, with solid body rotation at a fraction of the cone velocity. This occurs in regime I_b and, as shown later, also in regime II at small r . Eventually, for applied rates $\dot{\gamma}_a \geq 5$ s⁻¹, both in Fig. 3(c) and (d) the bulk of the sample starts to yield, $\dot{\gamma} > 0$. The difference between $\dot{\gamma}$ and $\dot{\gamma}_a$ decreases on increasing $\dot{\gamma}_a$ and the flow curve approaches bulk HB behavior.

The typical behavior described above, with the transition from a Bingham to a HB flow regime, is representative for all RI-matched suspensions with $\phi > 0.57$ and at least one smooth wall. We illustrate this in Fig. 4 and Fig. 5. The former shows the two-step Bingham

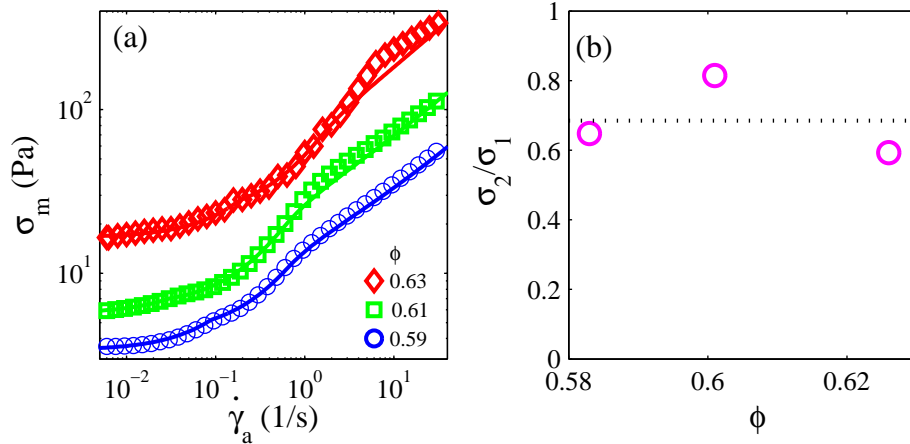


FIG. 4. (a) Flow curves for two uncoated surfaces, $a = 150$ nm, and various ϕ . The lower branches of the full lines are fits to Eqs. (10,11), the upper branch is Eq. A2 for slip at two surfaces. The parameters are $\sigma_{1,2} = [7, 5.7]$ Pa, $\beta = 19.0 \cdot 10^4$ Pa \cdot s \cdot m $^{-1}$, $\sigma_y = 23.5$ Pa, $\alpha = 18.0$ Pa \cdot s $^{1/2}$ for $\phi = 0.61$ and $\sigma_{1,2} = [28, 16.6]$ Pa, $\beta = 26.3 \cdot 10^4$ Pa \cdot s \cdot m $^{-1}$, $\sigma_y = 82$ Pa, $\alpha = 50.6$ Pa \cdot s $^{1/2}$ for $\phi = 0.63$ (the $\phi = 0.59$ parameters are as in Fig. 3b). (b) Ratio of the slip threshold stresses at the bottom and top surface, σ_2/σ_1 , versus ϕ , the dotted line is the average value.

behavior for two uncoated walls, as in Fig. 3(b) but now including two other concentrations. Both the slip threshold stress (σ_1 for the cone, σ_2 for the plate) and σ_y increase strongly with ϕ . Figure. 4(b) shows that the ratio between the slip threshold stress for the two surfaces is essentially independent of ϕ . In Fig. 5 we show $(\sigma - \sigma_s)/\eta_{\text{eff}}$ versus applied shear rate for suspensions with $a = 138$ nm at various ϕ , using a coated cone and smooth glass plate. Plotted this way, all curves at small $\dot{\gamma}_a$ (regime I) are linear and overlap, following Eq. (1). In addition to the threshold stress, also the fitted values of the Bingham viscosity show a strong ϕ -dependence, both of which are discussed in Sec. VI.

Figure 6(a) shows velocity profiles from the experiment in Fig. 3(a) ($\phi = 0.59$, coated cone, uncoated plate), but at a constant applied shear rate $\dot{\gamma}_a = 1.1$ s $^{-1}$, at various distances r . For this applied rate, σ_m is close to its value measured in the absence of slip (see Fig. 3(a)), but slip is nevertheless visible. For large r , slip and bulk flow are simultaneously present, the mechanism governing slip in regime I thus persists when bulk shear is present. The slip gets more pronounced for smaller r , which is shown directly in Fig. 6(b) via the r -dependence of the local shear rate $\dot{\gamma}(r)$ extracted from Fig. 6(a): $\dot{\gamma}(r)$ decreases strongly with r and eventually vanishes completely for $r < r_y \simeq 2.5$ mm, with r_y a “yielding radius” inside of

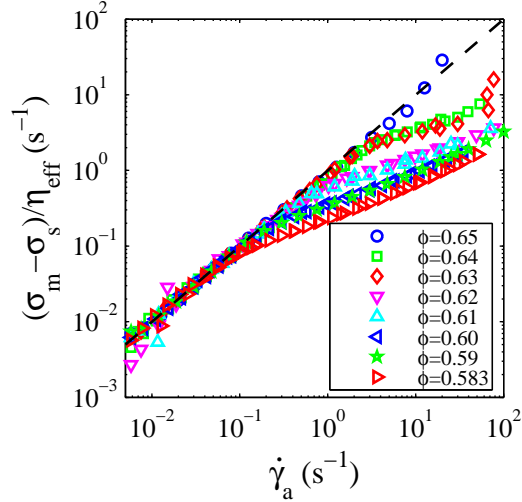


FIG. 5. Shear stress minus slip stress $\sigma_s(\phi)$ divided by the Bingham viscosity $\eta_{\text{eff}}(\phi)$ for $a = 138$ nm and $\phi = 0.585\text{--}0.65$. σ_s and η_{eff} were extracted from fits of the small $\dot{\gamma}_a$ behavior to Eq. (1). Dashed line: $\sigma_m - \sigma_s = \dot{\gamma}_a \eta_{\text{eff}}$.

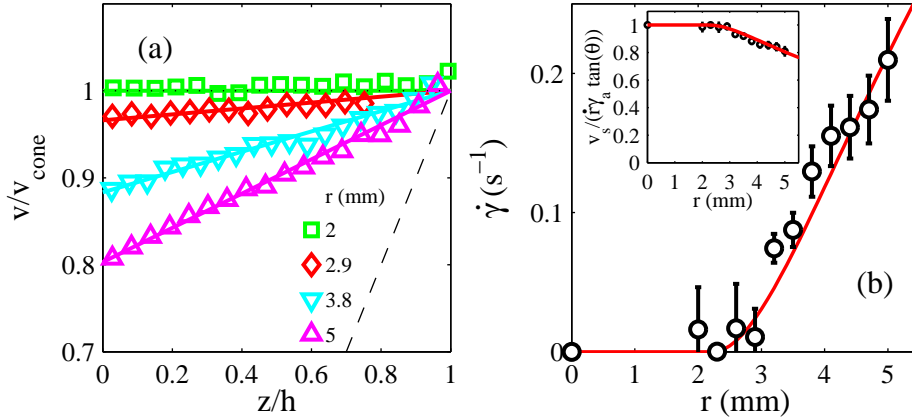


FIG. 6. (a) Velocity profiles for fixed shear rate $\dot{\gamma}_a = 1.1 \text{ s}^{-1}$, $\phi = 0.59$ and $a = 138$ nm with uncoated glass and coated cone, at selected distances r from the center. (b) Corresponding local shear rate versus r . Full line: Eq. (5) with $h = r \tan(\theta)$, using Eq. (6) and rheological parameters as in Fig. 3(a). Inset: corresponding r -dependence of the normalized slip velocity $\tilde{v}_s = v_2/(\dot{\gamma} r \tan \theta)$, along with the prediction using Eqs. (4),(5) and (6) with $v_1 = 0$ (full line).

which no shear is present. These data demonstrate directly that, in presence of slip, the stress in a cone-plate, while essentially uniform across the gap, is radially non-uniform: for small r , $\sigma(r) < \sigma_y$, while for larger r , $\sigma(r) > \sigma_y$.

The velocity profiles at small $\dot{\gamma}_a$ in Figs. 3 suggest that in regime I the suspension moves as a solid body, without bulk shear, down to the glass plate. To get direct evidence for this and exclude locally non-uniform flow as seen in colloidal crystals [Derks *et al.* (2004); Cohen *et al.* (2006)], we imaged the first layers of a suspension of fully fluorescent particles ($a = 652$ nm) in regime I in the RI-matching solvent. As reported in Fig. 2a of [Ballesta *et al.* (2008)], in regime I below the critical applied shear rate $\dot{\gamma}_{a,c}$ mentioned earlier, we observed plug flow with $v_s = v_{cone}$ down to the first layer of particles. There is thus no highly sheared layer of colloids and the Bingham slip response, Eq. 1, reflects the behavior of a lubrication layer between the first particles and the wall. Due to the smooth wall, the colloids do exhibit some layering at the surface, but this vanishes completely beyond ~ 4 particle diameters (Fig. 2a of [Ballesta *et al.* (2008)]), where the structure is that of a fully disordered colloidal glass. Even near the wall, no significant ordering was observed within the imaging plane.

IV. MODEL FOR THE SLIP AND YIELD BEHAVIOR

The local and global rheology in the previous section can be described via a model based on the same assumption used in [Yoshimura and Prud'homme (1988); Russel and Grant (2000); Kalyon (2005)], i.e. that the stress at the wall due to slip matches the stress in the bulk. As suggested by the phenomenology of the smooth wall flow curves, Fig. 3(a),(b) and the Bingham form Eq. 1 for the slip branch, the local stress σ_{slip} and the slip velocity v_i of the colloids along a wall, labeled by i , can be related via:

$$\sigma_{\text{slip}} = \sigma_i + \beta_i v_i. \quad (2)$$

Here $\beta_i v_i$ is a hydrodynamic term reflecting the lubrication between the first layer of colloids and the wall and the threshold stress σ_i is similar to a Coulomb friction term. Unless particles strongly interact with one of the smooth surfaces the mean distance of a particle to the surface will mostly be determined by the available free space, which only depends on ϕ ; hence we assume that $\beta_1 = \beta_2 = \beta(\phi)$. On the other hand we expect σ_i to depend on the wall interaction which can differ between the surfaces. A more detailed description of these terms will be given later. Below we use the convention $i = 1$ for the top surface, $i = 2$ for the bottom plate and also assume that $\sigma_1 \geq \sigma_2$.

For the bulk flow, we use the HB form, taking for simplicity an exponent $n = 0.5$:

$$\sigma_{\text{bulk}} = \sigma_y + \alpha \dot{\gamma}^{0.5}. \quad (3)$$

Although the measured n can vary ($0.35 \lesssim n \lesssim 0.6$) for $1 \gtrsim \phi/\phi_{rcp} \gtrsim 0.85$, as long as $n < 1$ the results below remain qualitatively correct. The relative contribution of slip and flow is then evaluated via $\sigma_{\text{bulk}} = \sigma_{\text{slip}}$ along with the relation between $\dot{\gamma}$ and $v_{1,2}$:

$$h\dot{\gamma} + v_1 + v_2 = h\dot{\gamma}_a. \quad (4)$$

Due to the dependence on the gap size h , the results are geometry dependent. We illustrate this for infinite parallel plates and the cone-plate geometry.

A. Infinite parallel plates

This idealized situation serves as the basis for subsequent analysis of the cone-plate geometry. Various cases are possible depending on the relative values of σ_s , σ and σ_y . We first consider the case $\sigma < \sigma_y$. In this regime bulk shear is absent, $\dot{\gamma} = 0$. For $\sigma_2 \leq \sigma < \sigma_1, \sigma_y$ (regime I or I_a) slip is localized at one surface, leading to $\sigma = \sigma_2 + \beta h \dot{\gamma}_a$. For $\sigma_1, \sigma_2 \leq \sigma < \sigma_y$ (regime I_b) the sample slips at both surfaces and we have $\sigma = (\sigma_1 + \sigma_2)/2 + \beta h \dot{\gamma}_a/2$.

Whenever $\sigma_2 < \sigma_y$, yielding sets in at a slip velocity $v_2 = (\sigma_y - \sigma_2)/\beta$. This defines the transition from regime I or I_b to regime II, where bulk flow and slip coexists. The relation $\dot{\gamma}(\dot{\gamma}_a)$ is obtained by equating Eqs. (2) and (3), using Eq. (4). For slip at one wall ($v_1 = 0$, $\sigma_2 \leq \sigma_y \leq \sigma < \sigma_1$), this gives:

$$\dot{\gamma} = \dot{\gamma}_a - \dot{\gamma}_y + \dot{\gamma}_0 \left(1 - \sqrt{1 + \frac{2}{\dot{\gamma}_0} (\dot{\gamma}_a - \dot{\gamma}_y)} \right), \quad (5)$$

$$\Delta\sigma = \sigma_y - \sigma_2, \quad \dot{\gamma}_y = \frac{\Delta\sigma}{\beta h}, \quad \text{and} \quad \dot{\gamma}_0 = \frac{\alpha^2}{2h^2\beta^2}. \quad (6)$$

For $\sigma_{1,2} < \sigma_y < \sigma$, the sample yields and slips at both surfaces. The relation $\dot{\gamma}(\dot{\gamma}_a)$ is still given by Eq. (5), with:

$$\Delta\sigma = \sigma_y - \frac{\sigma_1 + \sigma_2}{2}, \quad \dot{\gamma}_y = \frac{2\Delta\sigma}{\beta h}, \quad \text{and} \quad \dot{\gamma}_0 = \frac{2\alpha^2}{h^2\beta^2}. \quad (7)$$

Equation (5) can be written in dimensionless form, giving the following master curve for the local shear rate versus applied rate in regime II:

$$\dot{\Gamma} = 1 + \Omega - \sqrt{1 + 2\Omega}, \quad (8)$$

with $\dot{\Gamma} = \dot{\gamma}/\dot{\gamma}_0$ and $\Omega = (\dot{\gamma}_a - \dot{\gamma}_y)/\dot{\gamma}_0$, in which the h dependence is absorbed. This form describes the vanishing bulk shear rate for $\dot{\gamma}_a \rightarrow \dot{\gamma}_y$ and the approach towards the HB curve ($\dot{\gamma} \rightarrow \dot{\gamma}_a$) for large rate. This can also be described in terms of the slip length l_s , see App. A 3; entering regime II, l_s decreases and approaches $l_s \sim \dot{\gamma}^{-1/2}$ for large $\dot{\gamma}_a$.

B. Cone and plate

To analyze the cone-plate geometry, the variation in gap size needs to be accounted for. Approximating the geometry at a distance r by parallel plates, the local stress is deduced as before, with $\sigma(r) = \sigma(h/\tan(\theta), \dot{\gamma}_a)$. The measured stress σ_m is found by integrating $\sigma(r)$ over the entire geometry:

$$\sigma_m = \frac{1}{\pi r_c^2} \int_0^{r_c} \sigma(r) 2\pi r dr. \quad (9)$$

We again first consider the case $\sigma(r) < \sigma_y$, i.e. solid body rotation of the entire sample ($\dot{\gamma} = 0$ for all r). In regime I or I_a, where slip occurs at the plate ($\sigma_2 \leq \sigma < \sigma_1, \sigma_y$) we have:

$$\sigma_m^I = \sigma_2 + 2\beta \tan(\theta) r_c \dot{\gamma}_a / 3. \quad (10)$$

which is the Bingham form Eq. (1) with $\eta_{\text{eff}} = 2\beta \tan(\theta) r_c / 3$. For complete slip at two surfaces $\sigma_1, \sigma_2 \leq \sigma < \sigma_y$, regime I_b, the solid body rotation rate of the sample is reduced, see Eq. (A5) in App. A 2. The stress is obtained from a balance of the total stress on the bottom plate and the cone (App. A 2):

$$\sigma_m^{\text{Ib}} = (\sigma_1 + \sigma_2) / 2 + \beta \tan(\theta) r_c \dot{\gamma}_a / 3. \quad (11)$$

The transition I_a \rightarrow I_b occurs when $\sigma_m^{\text{Ia}} = \sigma_m^{\text{Ib}}$ giving Eq. (A6) in App. A 2.

Due to the non-uniform slip velocity and associated nonuniform stress, the yielding transition and flow in regime II differ from that for parallel plates. For slip at the bottom plate ($\sigma_1 = \infty, v_1 = 0$), when increasing $\dot{\gamma}_a$, yielding starts when $\sigma_{\text{slip}} = \sigma_y$, i.e. at a radius $r_y = (\sigma_y - \sigma_2) / (\beta \tan(\theta) \dot{\gamma}_a)$. The applied rate where regime II starts follows from $r_y = r_c$:

$$\dot{\gamma}_{a,c} = (\sigma_y - \sigma_2) / \beta r_c \tan(\theta) \quad (12)$$

For $\dot{\gamma}_a > \dot{\gamma}_{a,c}$, the boundary between solid body rotation ($r < r_y$) and slip and shear ($r > r_y$) moves inward. The measured stress in regime II follows from Eq. 9 integrated over these two regions. The result, Eq. (A2) in App. A 1 is shown for specific parameters in Fig. 7, along

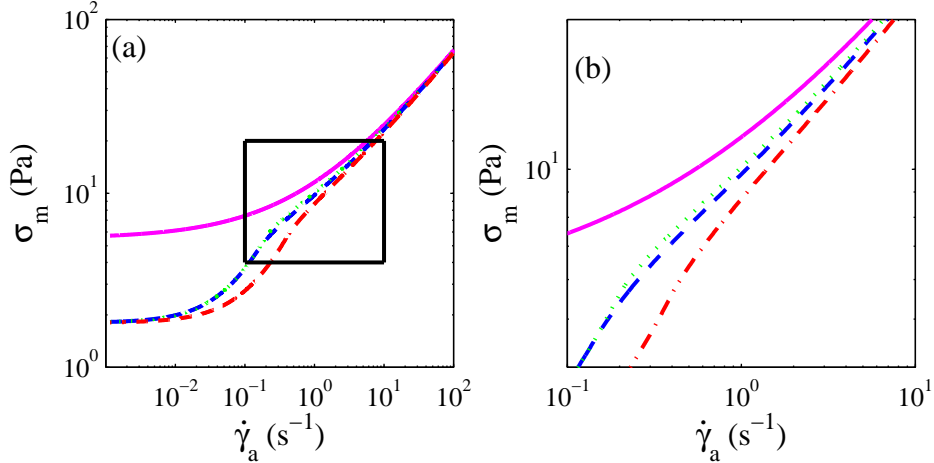


FIG. 7. (a) Full line: HB flow curve with $n = 0.5$, $\alpha = 6.1 \text{ Pa}\cdot\text{s}^{-0.5}$, and $\sigma_y = 5.5 \text{ Pa}$. Other curves: calculations for different geometries with slip at the bottom plate using $\beta = 82000 \text{ Pa}\cdot\text{s}/\text{m}$, $\sigma_s = 1.8 \text{ Pa}$: cone-plate with $\theta = 1^\circ$, $r_c = 20 \text{ mm}$ (dashed line, Eqs. (10,A2)); parallel plate with $h = 2 \tan(\theta)r_c/3$ (dotted) and $h = \tan(\theta)r_c/3$ (dash-dot), using Eqs. (3,5,6). (b) Zoom in on (a).

with that for parallel plates for two different gaps. The transition I-II for the cone-plate is smoother than for parallel plates due to the 'mixed' nature of the transition in the former.

For slip at two surfaces, the transition to regime II is somewhat more complicated due to a small difference in $\sigma(r)$ between bottom plate and cone in regime I. Yet, with the approximation $\sigma_1 - \sigma_2 \ll \sigma_y$ the analysis is essentially the same as for slip at one surface, see App. A2: the transition to regime II is described by Eq. (12) with the substitution $\sigma_2 \rightarrow (\sigma_1 + \sigma_2)/2$ and $\beta \rightarrow \beta/2$.

V. COMPARISON WITH EXPERIMENT

A. Global rheology

The uniform lubrication layer and solid body rotation in regime I lead to an effective viscosity $\eta_{\text{eff}} \sim \beta r_c \tan(\theta)$, which can be verified by comparing slip branches for different cones. Figure 8(a) shows results for coated cones with different r_c and θ and uncoated glass plate for the same sample ($a = 138 \text{ nm}$, $\phi = 0.63$). The data for $r_c = 20 \text{ mm}$, $\theta = 2^\circ$ and $r_c = 10 \text{ mm}$, $\theta = 4^\circ$ indeed superimpose for all $\dot{\gamma}_a$, as all geometry dependence of σ_m in regime I and II (Eq. (A2)) enters via $r_c \tan(\theta)$. When plotted versus the velocity at the edge

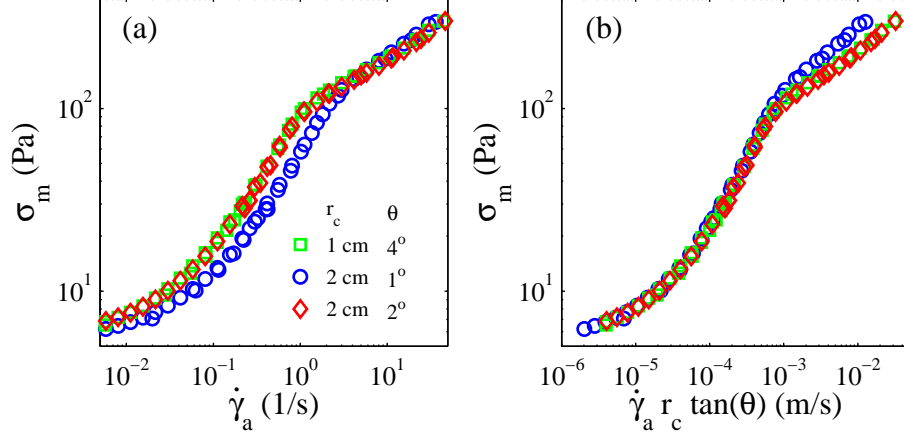


FIG. 8. (a) Flow curves for an RI-matched suspension with $a = 138$ nm, $\phi = 0.63$, using different coated cones and smooth plates. (b) σ_m versus velocity at the geometry edge; symbols as in (a).

of the geometry, $\dot{\gamma}_a r_c \tan(\theta)$, Fig. 8(b), all slip branches superimpose.

The transition from Bingham slip to HB bulk flow behavior in the global flow curves is well described by Eqs. (10, 11) and (A2). The parameters α , σ_y and β and $\sigma_{1,2}$ entering Eq. (A2) (for regime II) follow from fits of the global rheology with and without coating. Examples of the predicted full flow curves are shown in Fig. 3(a)(b) and Fig. 4. In Fig. 3(a) the measured transition from regime I to II for one smooth wall is well captured. In Fig. 3(b) and 4, where both walls are uncoated, the transition from slip at one surface to two surfaces and the subsequent yielding are also well described. The small discrepancy for $\phi = 0.63$ can be attributed to both a slight reduction of the HB exponent $n < 0.5$ for the largest ϕ and the presence of shear localization near the yield stress in this ϕ regime, see Sec. VII.

B. Local shear rate

The model can be checked further by comparing flow profiles to the predictions for local shear rate and slip velocities in Sec. IV. To obtain these quantities, $v(z)$ is fitted to $v = \dot{\gamma}z + v_s$. Figure 9(a),(c) shows the reduced bulk rate $\dot{\gamma}/\dot{\gamma}_a$ and slip velocity v_s at the plate from $v(z)$ taken at $r = 2.5$ mm (shown in Fig. 3(c)) and $r = 4$ mm. As expected from Eq. (5), bulk shear starts at smaller $\dot{\gamma}_a$ for larger r , hence for $r < r_c$ the solid body rotation extends beyond the transition rate $\dot{\gamma}_{a,c} \simeq 0.135$ s $^{-1}$ given by Eq. (12). Similarly Fig. 9(b-d-e) presents the local bulk rate and slip velocities $v_1(\dot{\gamma}_a)$, $v_2(\dot{\gamma}_a)$ for uncoated cone and plate

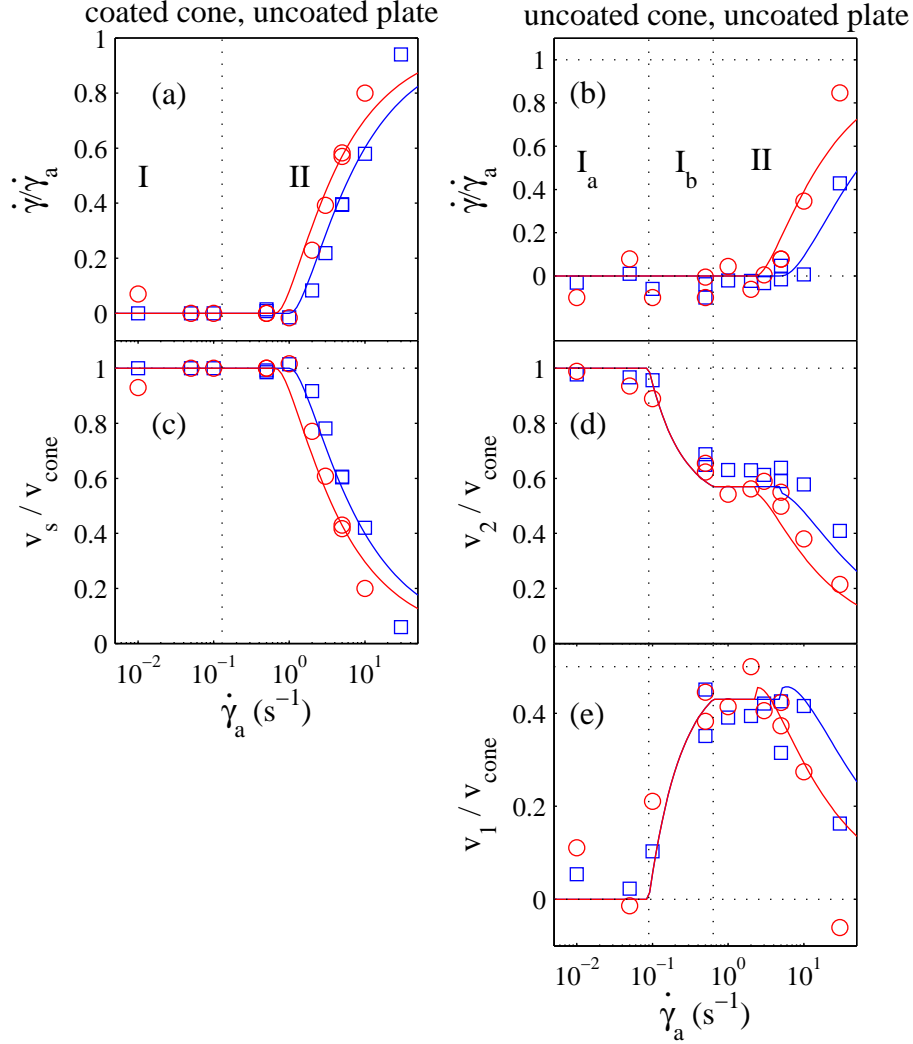


FIG. 9. Velocimetry results corresponding to the data in Fig. 3. (a),(b) Measured normalized local shear rate versus $\dot{\gamma}_a$ for (a) $r = 2.5$ mm (\square) and $r = 4$ mm (\circ), and (b) $r = 2.5$ mm (\square) and $r = 5.5$ mm (\circ). (c),(d) Normalized slip velocity v_s/v_{cone} at the glass plate corresponding to data in (a),(b). In (e) the normalized slip velocity at the cone is shown. Data in (a),(c) are for $a = 138$ nm, coated cone and uncoated plate. Data in (b),(d) and (e) are for $a = 150$ nm, uncoated cone and uncoated plate. Full lines in (a),(b) for $\dot{\gamma} > 0$ are given by Eqs. (5,6) and Eqs. (5,7), respectively, with parameters given in the caption of Fig. 3. In (d),(e), the curves in regime I_b are given by Eq. (A5); the transition $I_a \rightarrow I_b$ occurs at $\dot{\gamma}_a^*$ given in Eq. (A6). The bulk (slip) velocity at the second $v_{1,2}$ plateau (corresponding to $r < r_y$ in regime II) is given by Eq. (A7); In (c) and (d),(e) the curves for the largest $\dot{\gamma}_a$ (where $r > r_y$) follow from those in (a),(b) via Eq. (4).

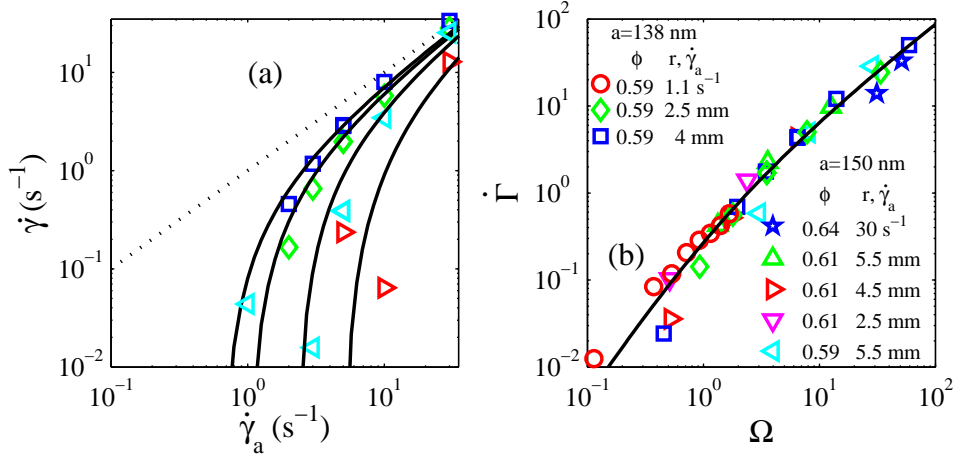


FIG. 10. (a) Local shear rate $\dot{\gamma}$ extracted from the measured $v(z)$, versus $\dot{\gamma}_a$ for different ϕ , a and r , see symbols in (b), for slip at the bottom plate only ($a = 138$ nm data) and at both surfaces ($a = 150$ nm data). The full lines represent Eq. (5) with the rheological parameters entering via Eq. (6) or Eq. (7) with $h = r \tan(\theta)$. Dotted line: $\dot{\gamma} = \dot{\gamma}_a$. (b) Normalized local shear rate $\dot{\Gamma}$ versus normalized applied rate Ω for various r , ϕ and two particle sizes. The full line shows Eq. (8).

taken at $r = 5.5$ mm (from Fig. 3(d)) and at $r = 2.5$ mm. Both the transition from regime I_a to I_b and that to regime II are well described. Due to the small difference between the slip stresses σ_1 and σ_2 for bottom and top, the extent of regime I_b is limited. Note that v_1 and v_2 are essentially constant between $\dot{\gamma}_{a,c}$ and $(2\sigma_y - \sigma_1 - \sigma_2)/\beta r \tan(\theta) \simeq 4 - 7$ s $^{-1}$, which motivated the simplification of the model for two uncoated plates in App. A2. For $\dot{\gamma}_a \gtrsim 4 - 7$ s $^{-1}$, the bulk shear rate $\dot{\gamma}$ and $v_{1,2}$ also match the predictions.

The radial variation of $\dot{\gamma}$ over the geometry in regime II, shown in Fig. 6(b), is also well explained by the model. The line in Fig. 6(b) shows that both the onset of yielding at $r_y \simeq (\sigma_y - \sigma_s)/(\beta\theta\dot{\gamma}_a) = 2.35$ mm and the r -dependence of the bulk shear rate directly follow from the measured rheological parameters. Finally, in Fig. 10(a) we show $\dot{\gamma}$ versus $\dot{\gamma}_a$ for different ϕ and particle sizes along with the model predictions (see caption). Using the normalization described below Eq. 8, $\dot{\Gamma} = \dot{\gamma}/\dot{\gamma}_0$ and $\Omega = (\dot{\gamma}_a - \dot{\gamma}_y)/\dot{\gamma}_0$, all data indeed collapse on the master curve $\dot{\Gamma} = 1 + \Omega - \sqrt{1 + 2\Omega}$, Fig. 10(b). Overall, both macroscopic and microscopic observations thus validate the phenomenological model.

VI. ANALYSIS OF BULK FLOW AND SLIP PARAMETERS

Before discussing the nature of the slip behavior, we first present the bulk rheological parameters, measured in detail for the $a = 138$ nm and $a = 150$ nm samples using rough, coated walls. Figure 11(a) shows that σ_y , plotted as function of the normalized distance to random close packing, strongly increases towards rcp and is reasonably described by $\sigma_y a^3/k_B T \simeq 0.01(1 - \phi/\phi_{rcp})^{-3}$. This increase of σ_y is due to tightening of particle cages and strongly increasing entropic barriers. The HB exponent n , Fig. 11(b), is in the range $0.4 - 0.55$ with a slightly decreasing trend for $\phi \rightarrow \phi_{rcp}$ ³. Further, the HB parameter α also strongly increases with ϕ , Fig. 11(c), following approximately $\alpha \propto (1 - \phi/\phi_{rcp})^{-2.5} \simeq (1 - \phi/\phi_{rcp})^{n-p}$. This implies the following scaling of the bulk HB rheology:

$$\sigma = \sigma_y + \alpha \dot{\gamma}^n = \sigma_y(\phi)[1 + A(1 - \phi/\phi_{rcp})^n (\dot{\gamma} \tau_B)^n] = \sigma_y(\phi)[1 + A(\dot{\gamma} \tau_m(\phi))^n], \quad (13)$$

with $\tau_m = \tau_B(1 - \phi/\phi_{rcp})$ a characteristic microscopic ϕ dependent (in-cage relaxation)

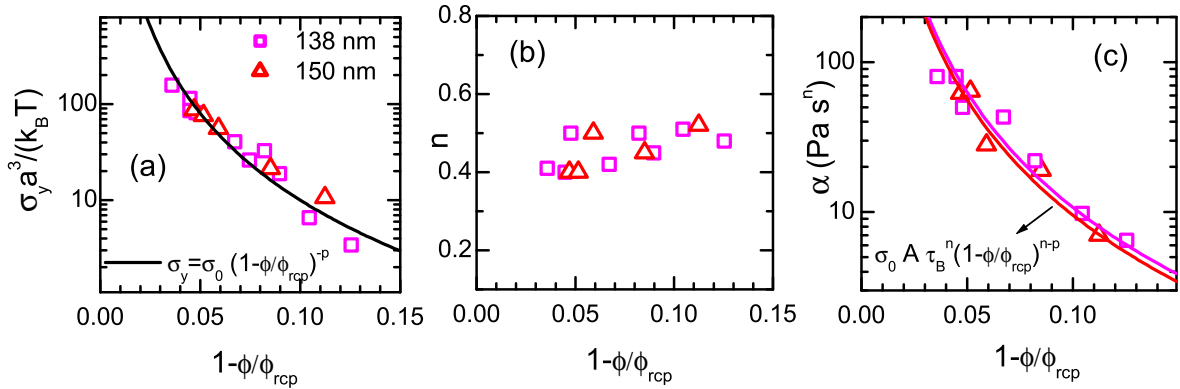


FIG. 11. Bulk HB parameters for $a = 138$ nm and $a = 150$ nm versus $1 - (\phi/\phi_{rcp})$. (a) Normalized yield stress. Line: $\sigma_y = \sigma_0 [1 - (\phi/\phi_{rcp})]^{-p}$ with $p = 3$ and $\sigma_0 = 0.01 k_B T / a^3$. (b) the HB exponent n . (c) The HB parameter α . Lines: $\alpha = A \sigma_0 \tau_B^n [1 - (\phi/\phi_{rcp})]^{n-p}$ with $A = 10$, $n = 0.45$, $p = 3$ and $\tau_B = 0.0285$ s and $\tau_B = 0.036$ s the Brownian times.

time scale in the glass, τ_B the Brownian time and A given by $A = \alpha / [\sigma_y \tau_B^n (1 - \phi/\phi_{rcp})^n]$.

³ These exponents do not necessarily reflect terminal slopes of $\log(\sigma_m)$ vs $\log(\dot{\gamma}_a)$. Somewhat larger values ($n \lesssim 0.65$) have also been observed in other PMMA HS suspensions [Koumakis *et al.* (2012)]

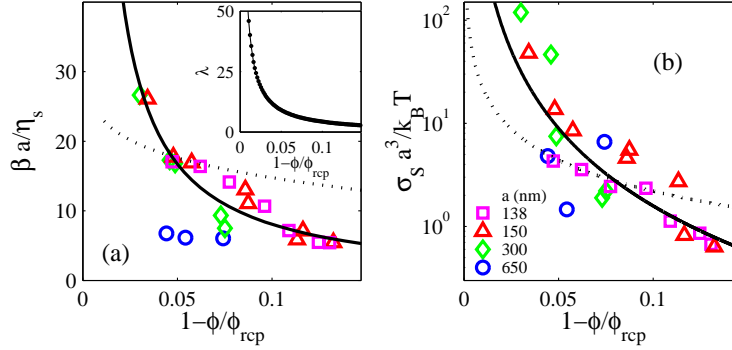


FIG. 12. (a) Normalized lubrication parameter $\beta a / \eta_s$ versus $1 - \phi / \phi_{rcp}$. Symbols: data for different particle size (see (b)); full line: result based on Eq. (17). Dotted line: result based on Eq. (14) and the explanation in the text. Inset: (\bullet) λ versus $1 - \phi / \phi_{rcp}$ from a numerical evaluation of Eq. (16). The full line represent $\lambda \propto \Pi / \Pi_0$. (b) Normalized slip stress $\sigma_s a^3 / k_B T$ versus $1 - \phi / \phi_{rcp}$, the dotted line is $\sigma_s = 0.45\Pi$, the full line represents Eq. (18) with $A = 0.005$ and $m = 2.5$.

While this phenomenological behavior has no solid theoretical basis, it is physically plausible and has been used successfully in [Besseling *et al.* (2010)]. We do not further pursue its interpretation here, but instead turn to the behavior of the slip parameters.

A. ϕ dependence for non-stick walls

As mentioned, for smooth, non-stick walls the Bingham slip parameters β and σ_s in Eq. (2) show a strong increase with ϕ . We show the parameters extracted from the rheology in Fig. 12(a),(b), where in (a) the lubrication parameter has been normalized by the solvent viscosity and particle size, while in (b) the stress is normalized by $k_B T / a^3$. We observe a characteristic increase of the parameters for $\phi / \phi_{rcp} \rightarrow 0$ for the different particle sizes, except for deviations for the $a = 652$ nm particles⁴.

We now attempt to rationalize this behavior in terms of the physical properties of the suspension and the (hard) interaction with the wall. We first discuss the lubrication parameter β . The linear increase of stress with velocity, Eq. (2), implies that β is governed by hydrodynamic friction between the first layer of particles and the wall, with an effective lubrication layer thickness independent of velocity. For a single particle of radius a , centered

⁴ The latter might be partly due to a somewhat reduced sediment volume fraction $\phi_{sed} < \phi_{rcp}$ from centrifugation of this batch (as discussed in Sect. II A), thus slightly overestimating of ϕ / ϕ_{rcp} .

at a distance $a + \delta$ from the wall, moving with constant velocity v in a solvent of viscosity η_s , the drag force it experiences is $\eta_s v a f(\delta)$, where $f(\delta/a) \simeq 18.1 - 10 \ln(\delta/a)$ for $\delta \ll a$. $f(\delta)$ reflects the wall induced hydrodynamic reduction of the particle mobility [Goldman *et al.* (1967)] for no-slip boundary conditions. For a distribution of particles with concentration $n(\delta)$ moving with respect to the wall, the mean stress on the wall follows from integrating over δ . The lubrication parameter $\beta = \sigma/v$ may thus be written in normalized form as:

$$\beta a / \eta_s = \sigma a / \eta_s v = \int_0^\infty a^2 f(\delta) n(\delta) d\delta. \quad (14)$$

We assume that beyond the first layer the fluid and colloids move together, hence the integral can be cut off at $\delta = a$. With the further assumption that solvent flow in the lubrication layer does not change the distribution $n(\delta)$ and that colloid interactions can be ignored, β may be evaluated from the “equilibrium” distribution $n_e(\delta)$. It was demonstrated in [Henderson and van Swol (1984)] that the contact value $n_e(0)$ follows $n_e(0) = \Pi/k_B T$ with Π the osmotic pressure of the suspension at rest. While $\Pi(\phi)$ is uncertain for $\phi > \phi_g$ ([Hermes and Dijkstra (2010), Phan *et al.* (1996), Tokuyama and Terada (2007)]), a widely used form is [Brady and Vivic (1995)]:

$$\Pi = 2.9\Pi_0/(1 - \phi/\phi_{rcp}), \quad \text{with} \quad \Pi_0 = 3\phi k_B T/(4\pi a^3). \quad (15)$$

Simulations for $\phi < 0.5$ in [Henderson and van Swol (1984)] further showed that in the first layer n_e decreases as $n(\delta) = n_e(0) \exp(-3\lambda\delta(1 + \delta/a + \delta^2/3a^2)/a)$, with λ a ϕ -dependent parameter. Employing this form also for the colloidal glass, $\lambda(\phi)$ can be extracted by equating ϕ in the first layer to the bulk value:

$$\frac{2\pi a^2}{3} \int_0^a n(\delta) d\delta = \phi \sim a^2 \int n_e(0) \exp(-\lambda\delta/a) d\delta \sim n_e(0) a^3 / \lambda \quad (16)$$

Numerical solution of the l.h.s. of Eq. 16 gives $\lambda(\phi) \propto \Pi(\phi)/(k_B T/a^3)$ (inset to Fig. 12(a)), as also confirmed by the scaling in the r.h.s. of Eq. 16. Using $\lambda(\phi)$ we then calculate β from Eq. 14. The result, shown by the dashed line in Fig. 12(a), is finite for all ϕ and diverges as $\phi \rightarrow \phi_{rcp}$, approximately as $\beta a / \eta_s \propto -\ln(1 - \phi/\phi_{rcp})$. While this qualitatively accounts for the data, and Eq. 14 matches the experimental $\beta \propto \eta a^{-1}$ scaling (Figs. 15 and 12(a)), the predicted $\beta(\phi)$ clearly does not properly describe the experimental results.

A possible explanation for the discrepancy is that the chosen form for $f(\delta)$ only applies for a single particle. However, while colloid interactions are known to limit the wall induced

reduction of diffusion in concentrated colloidal liquids [Michailidou *et al.* (2009)], recent simulations [Swan (2010)] show that for small δ the logarithmic $f(\delta)$ nevertheless holds. An alternative explanation is that the “equilibrium” form n_e does not correctly represent the near wall particle distribution. This can be due to the fact that already at rest the structure is out of equilibrium (since $\phi > \phi_g$), possibly combined with the layering or a change in concentration in the wall layer as observed in [Dullens and Kegel (2004)]. Equally likely is that $n(\delta)$ differs from n_e due to the actual flow present in the slip layer, similar to dilute systems [Polverari and van de Ven (1995)]. This non-equilibrium effect can be quantified by comparing the shear rate in the lubrication layer with the inverse timescale $1/\tau_m$ for “cage” exploration (discussed at the start of this section), via a “wall” Péclet number $\text{Pe}_w = \tau_m v_s / \xi = \tau_m (\sigma - \sigma_s) / \eta_s$ (ξ is a mean layer thickness discussed below). Here τ_m is estimated using the mean free particle space (also described below) and the short time diffusion coefficient [Brady (1996)] as $\tau_m = 3\tau_B [1 - \phi/\phi_{rcp}]$, in line with τ_m inferred from the ϕ -scaling of the bulk rheology at the start of this section. Using the Brownian time $\tau_B \gtrsim 30$ ms and $\sigma - \sigma_s \gtrsim 0.2$ Pa, we have $\text{Pe}_w = O(1)$ and larger for our data in the slip regime. Thus, during slip $n(\delta)$ is indeed expected to differ considerably from n_e [Brady (1993)], but further measurements are required to confirm this.

Empirically, the bulk of the experimental data are well described by the form:

$$\beta a / \eta_s \equiv a / \xi \simeq 0.9 / (1 - \phi / \phi_{rcp}) \simeq \Pi / 3.2 \Pi_0, \quad (17)$$

where the l.h.s. defines the mean lubrication layer thickness $\xi \propto 1/\Pi$. In fact, the mean spacing $\langle s \rangle$ between colloids in the bulk is estimated as $\langle s \rangle = a((\phi_{rcp}/\phi)^{1/3} - 1) \simeq (a/3)(1 - (\phi/\phi_{rcp}))$, hence the empirical form implies $\xi \simeq 3.4\langle s \rangle$. Using n_e to calculate ξ gives similarly $\xi = a^2 \int_0^a \delta n(\delta) d\delta \simeq 2a\Pi_0/\Pi \simeq 2\langle s \rangle$, but this form can also result from other distributions, different from the ‘equilibrium’ one. Overall, the analysis suggests that the non-equilibrium behavior in the lubrication layer underlies the behavior of $\beta(\phi)$. Note that our $\beta(\phi)$ matches the predicted ϕ dependence of the high frequency viscosity or inverse short time diffusion constant in concentrated suspensions [Brady (1996)], for which, to our knowledge, no experimental verification yet exist for $\phi \rightarrow \phi_{rcp}$.

Next we discuss the behavior of the slip threshold σ_s . As seen in Fig. 12(b), $\sigma_s \propto 1/a^3$, suggesting a relation to the osmotic pressure. In this context, σ_s and Π may be naively linked via a phenomenological Coulomb friction mechanism using $\sigma_s = \mu\Pi$ with μ the

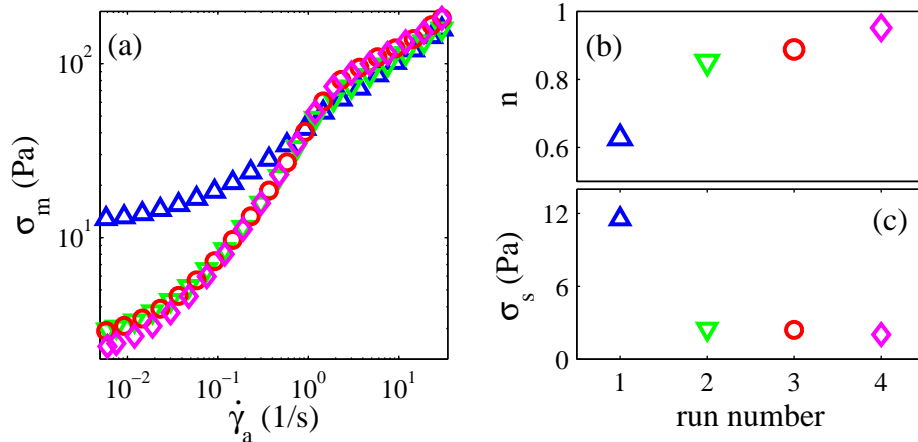


FIG. 13. (a) Measured stress σ_m versus $\dot{\gamma}_a$ for a suspension with $a = 138$ nm, $\phi = 0.61$ in RI-matching solvent, immediately after loading, going from small to large $\dot{\gamma}_a$ (Δ), followed by large to small $\dot{\gamma}_a$ (∇), again small to large (\circ) and finally large to small $\dot{\gamma}_a$ (\diamond). (b) The power m and (c) σ_s , both obtained from a fit of the low $\dot{\gamma}_a$ branch to $\sigma_m - \sigma_s \propto \dot{\gamma}_a^m$, versus run number.

friction coefficient. Comparing this with the data, we see that a value $\mu \simeq 0.45$ can describe σ_s at intermediate $1 - \phi/\phi_{rcp}$. Furthermore, recalling the experiments with two uncoated surfaces in Fig. 4, we found that the ratio between σ_s at the bottom plate and the cone is insensitive to ϕ , Fig. 4(b), which might support the Coulomb friction scenario. However, the overall ϕ dependence of the data in Fig. 12(b) is inconsistent with $\sigma_s \propto \Pi$ for constant μ . The data are considerably more scattered than for $\beta(\phi)$ and also exhibit unsystematic variation of σ_s within a factor 2 for different glass cleaning methods. While preventing a precise description of the divergence, the data are reasonably described by:

$$\sigma_s a^3 / k_B T \simeq A(1 - \phi/\phi_{rcp})^{-m}, \quad (18)$$

with $A \simeq 0.005$ and $m \simeq 2.5$. This dependence mimics the behavior of the yield stress, $\sigma_y a^3 / k_B T \simeq 0.01(1 - \phi/\phi_{rcp})^{-3}$. Thus, $\sigma_s/\sigma_y = O(0.1)$ and decreases weakly with ϕ as $\sigma_s/\sigma_y \simeq 0.5(1 - \phi/\phi_{rcp})^{0.5}$. Therefore $\sigma_s(\phi)$ may represent the stress required for the presumed reorganization of the particle distribution when slip sets in and the similarity between $\sigma_s(\phi)$ and $\sigma_y(\phi)$ could be connected to a similar change of the particle distribution due to 'cage' breaking for $\sigma = \sigma_y$.

A definite interpretation of σ_s is thus still lacking. We conclude by showing that nevertheless normal stresses in the system do seem to affect σ_s . For concentrated samples, the

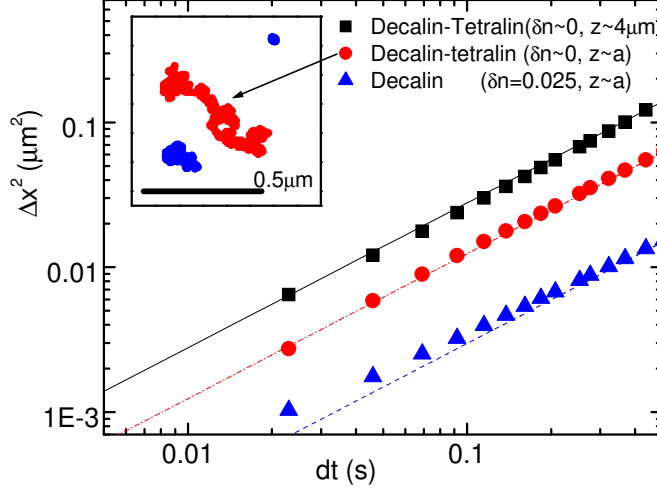


FIG. 14. Mean squared displacement of $a = 652$ nm particles versus time in dilute suspensions in a decalin-tetralin mixture far from the glass (\blacksquare), close to the glass (\bullet) and close to the glass in decalin (\blacktriangle). The lines represent diffusive behavior $\Delta x^2 = 2Dt$ with $D = 0.139 \mu\text{m}^2/\text{s}$, $D = 0.062 \mu\text{m}^2/\text{s}$ and $D = 0.014 \mu\text{m}^2/\text{s}$ from top to bottom. Inset: trajectories at $z \sim a$ of particles in decalin (the stuck particle and short trajectory) and a single long particle trajectory in decalin-tetralin (\bullet).

rheology of the system may show a transient behavior after initial sample loading, associated with local shear thickening behavior during loading. This is shown in Fig. 13 where a sample is submitted to repeated low-to-high-to-low shear rate cycles after loading. Fitting the low shear part of the first flow curve (\triangle) to $\sigma_m - \sigma_s \propto \dot{\gamma}_a^m$, we find $m \simeq 0.65$, i.e. in between the exponent 1 for Bingham slip and 0.5 for bulk flow, indicating a mixture of shear and slip. For the first run σ_s is significantly larger than for the next cycle(s), where both σ_s and m reach a constant value $\sigma_s \simeq 2$ Pa and $m \simeq 1$. Assuming that local shear thickened regions lead to relatively large local normal stresses, increasing σ_s , the reduced σ_s in repeat runs is consistent with flow induced relaxation of these local normal stresses.

B. Effect of wall interaction

As discussed, the slip response for HS glasses strongly depends on the colloid-wall vdW interaction ⁵. As shown in Fig. 2, for sufficient attraction slip vanishes, implying that the

⁵ Note that, generally, attractive colloid-wall forces alone do not guarantee elimination of slip. For e.g. flocculated gels, with a heterogeneous network of aggregates, a smooth, attractive (or even particle coated) wall can act as an easy ‘fracture’ plane resulting effectively in slip [Buscall *et al.* (1993)]. In these cases larger scale wall roughness - of the order of the aggregate size - is needed to prevent slip.

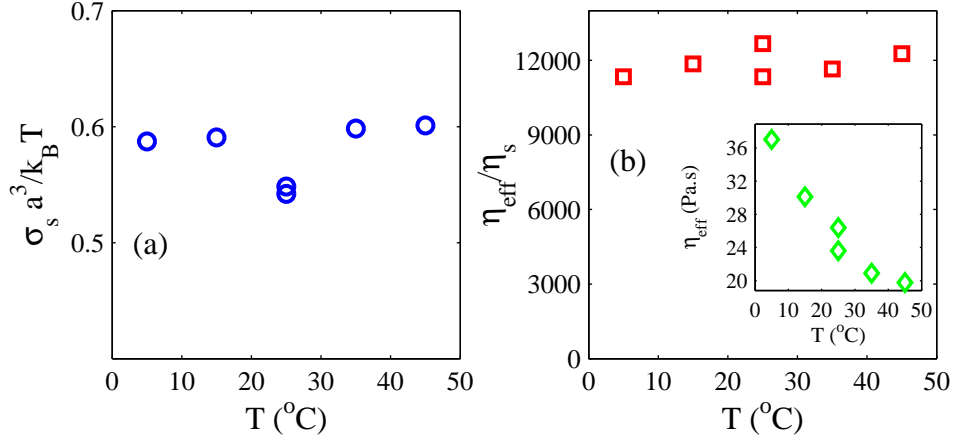


FIG. 15. Temperature dependence of (a) the normalized Bingham slip stress and (b) Bingham viscosity $\eta_{\text{eff}}(T)$ normalized by the temperature dependent solvent viscosity $\eta_s(T)$. Data are for $\phi = 0.59$, $a = 138$ nm using a coated cone and smooth glass. The inset to (b) shows the unrenormalized data $\eta_{\text{eff}}(T)$.

slip threshold stress $\sigma_s > \sigma_y$. To characterize directly the attraction, we imaged dilute suspensions of the $a = 652$ nm particles and analyzed the near-wall motion both in RI-matching and RI-mismatching solvents, without flow. In Fig. 14 we show the mean squared displacements (MSD) for the two cases, for particles imaged at the surface (i.e. $z \simeq a$ within the microscope z - resolution) and the MSD away from the surface. As expected, [Goldman *et al.* (1967); Sharma *et al.* (2008); Michailidou *et al.* (2009)] the MSD is smaller close to the wall than in the bulk. Moreover, with RI-matching the near wall MSD is five times larger than in the RI-mismatching solvent; in the latter case particles are (temporarily) stuck to the surface, evidencing the vdW attractions. With RI-matching the mobility is enhanced, vdW forces are reduced and insufficient to stick particles to the surface.

Even though the vdW interaction is strongly reduced by RI-matching, it cannot be completely suppressed. To study the role of remaining vdW forces on the slip stress σ_s (see Eq. 1), we have measured flow curves on the same sample, with smooth glass and coated cone, at various temperatures T . Changing T changes the RIs (mainly of the solvent) and might thus be observable in the dependence of σ_s on T . For all temperatures measured (5 – 45 C°) the flow curves exhibited the Bingham slip branch (data not shown), from which we extracted $\sigma_s(T)$ and the effective viscosity $\eta_{\text{eff}}(T)$ via Eq. 1. Figure 15(a) shows that the normalized slip stress, $\sigma_s a^3 / k_B T$, is nearly temperature independent, but exhibits

a small drop of $\sim 10\%$ for $T = 25^\circ\text{C}$. For decalin $\partial_T n_R = -4.4 \cdot 10^{-4} \text{ K}^{-1}$, introducing a temperature dependent solvent refractive index n_R in the calculations presented in App. B can be used to obtain a T -dependent particle-wall interaction. For what interests us here, there is a temperature interval where $n_{\text{PMMA}} < n_{\text{R,solvent}} < n_{\text{R,glass}}$ and thus colloid-wall interactions may become slightly repulsive (see Table 3 below). The observed minimum of σ_s can qualitatively be associated with such slight repulsion, although a calculation suggests that this should occur around 40°C rather than 25°C as observed experimentally (figure 15(a)). We attribute the difference to the approximations made in the calculation of the vdW interactions (App. B). Overall, we conclude that vdW forces do affect σ_s but, in the range of RI-mismatch considered here, have only a modest effect. The data for the Bingham viscosity $\eta_{\text{eff}}(T)$, inset to Fig. 15(b), also provide useful information. While $\eta_{\text{eff}}(T)$ exhibits a clear temperature variation, when normalized by the temperature dependent solvent viscosity, $\eta_s(T)$ no T dependence is detected (Fig. 15(b)) suggesting that the viscous slip is due to a lubrication layer of pure solvent between the colloids and the wall.

Rheology experiments along with near-wall motion measurements evidenced that sufficiently strong vdW attraction between colloids and walls suppresses slip in the HS glasses even with smooth walls. Changing the index matching influences both the vdW interaction between two particles and the particle-wall interaction. We calculated the interaction V_{pw} between the wall and a colloid of radius a separated by a distance δ , and the interaction energy V_{pp} between two colloids separated by a distance 2δ using the formulas in App. B. The parameters for each solvent are given in table II. The resulting particle-particle and particle-wall interactions for the various a and the different solvents are shown in table III using $\delta = 10 \text{ nm}$ as thickness of the steric layer. In decalin, particle-particle vdW attractions are weaker than $k_B T/10$ and thus can be neglected. However, the particle-wall (glass) vdW attraction is of the order of $k_B T$ for the larger particles explaining the significant tendency of these particles to stick to the surface, although such attractions are clearly weaker than $k_B T/10$ for smaller particles. Finally, the vdW attraction between colloids and the metallic cone is stronger than $k_B T$ for all particle sizes suggesting that a layer of stuck particles at the cone should be expected. In decalin-tetralin mixture all attractions are at least an order of magnitude smaller than $k_B T$. Hence in index matching solvent particle-particle and particle-wall interaction are reduced to their hard sphere counterparts.

Still, even with a good index matching, some residual van der Waals forces are present

Component	decalin	decalin-tetralin	PMMA	swollen PMMA	glass
n_R	1.47	1.51	1.49	1.51	1.523
ϵ	2.43	2.63	2.6	2.6	3.4

TABLE II. Dielectric permittivity ϵ and index of refraction n_R for the solvents, glass, and PMMA.

(see table III). Moreover, in decalin-tetralin mixtures, the particle-glass surface interaction is positive, which denotes a repulsive force. This is due to the fact that in this case $\epsilon_1 < \epsilon_3 < \epsilon_2$ (see table II). Even if such a repulsive interaction should enhance slip, the small energies involved allow us to mostly neglect this effect. Two other factors that can affect the slip parameter by modifying the friction coefficient are the variations of the index-matching solvent composition and the polymer stabilizing layer between different batches and particles, and the glass plates that are replaced in each measurement. These factors may introduce some experimental uncertainty resulting in a variation of σ_s by up to a factor of 2 between two different experiments. Thus, the friction coefficient may vary both for different particle sizes and between different experiments with the same sample.

sample name	asm340	asm247	asm209	asm195
a (nm)	138	150	300	652
$V_{pp}^{dec} (k_B T)$	-0.011	-0.012	-0.032	-0.082
$V_{pw}^{dec} (k_B T)$	-0.099	-0.11	-0.24	-0.55
$V_{pp}^{mix} (k_B T)$	-67 e-7	-76e-7	-20 e-6	-51 e-6
$V_{pw}^{mix} (k_B T)$	0.00097	0.0011	0.0024	0.0054
$V_{p-steel}^{dec} (k_B T)$	-4.58	-5.05	-11.1	-25.4
$V_{p-steel}^{mix} (k_B T)$	0.0076	0.0084	0.018	0.042

TABLE III. van der Waals interactions for different particle sizes a , surfaces and solvents: particle-particle interaction in decalin V_{pp}^{dec} , particle-wall interaction in decalin V_{pw}^{dec} , particle-particle interaction in decalin-tetralin V_{pp}^{mix} , particle-wall interaction in decalin-tetralin V_{pw}^{mix} , as well as the particle-steel cone interaction for decalin ($V_{p-steel}^{dec}$) and for decalin-tetralin ($V_{p-steel}^{mix}$).

VII. SHEAR LOCALIZATION

So far we have focused on results for which, at a given r (i.e. gap size) the shear rate $\dot{\gamma}(z)$ is essentially uniform over the gap when the suspensions start to yield. However, in experiments where slip is suppressed by coating both cone and plate, we have observed shear banding for small shear rates (near σ_y) and large ϕ . An example is shown in Fig. 16(a). For large rates, $v(z)$ is approximately linear, but for $\dot{\gamma} \leq 3 \text{ s}^{-1}$ the profiles become strongly nonlinear, with shear localization detected near the walls and a vanishing shear rate in the bulk for the smallest γ_a . In [Besseling *et al.* (2010)], we have shown that this behavior, with a *continuous* variation of $\dot{\gamma}(z)$ over the gap, can be explained by very small concentration gradients ($\delta\phi \lesssim 0.003$), caused by a dilation-like flow instability due to shear concentration coupling (SCC) [Schmitt *et al.* (1995)]. This is qualitatively different from other soft glasses [Besseling *et al.* (2010)] and cannot be explained using earlier models for heterogeneous glassy flow, e.g. involving specific wall rheology [Bocquet *et al.* (2009)]. This instability and the associated nonlinearity in $v(z)$ sets in below a typical rate $\dot{\gamma}_c(\phi)$ which becomes appreciable only for large ϕ .

While localization is most easily observed for coated walls, where the average bulk shear rate $\langle \dot{\gamma} \rangle = [v(z_g) - v(z = 0)]/z_g$ equals $\dot{\gamma}_a$, we have also detected nonlinear profiles for smooth walls near the slip to yield transition, $\langle \dot{\gamma} \rangle \rightarrow 0$, for large ϕ , Fig. 16(b). For $\dot{\gamma}_a = 3 - 5 \text{ s}^{-1}$ the suspension has started to yield, i.e. $\langle \dot{\gamma} \rangle > 0$, but the $\dot{\gamma}(z)$ is strongly reduced (enhanced) near the smooth (rough) wall compared to $\langle \dot{\gamma} \rangle$. Indeed, for $\dot{\gamma}_a = 5 \text{ s}^{-1}$ the mean shear rate is $\langle \dot{\gamma} \rangle \sim 0.2\dot{\gamma}_a = 1 \text{ s}^{-1}$, similar to the value of $\dot{\gamma}_a$ below which banding becomes significant for rough walls, Fig. 16(a). Due to such nonlinear flow near yielding, it is difficult to determine σ_y very precisely for $\phi/\phi_{rcp} \gtrsim 0.94$. The slightly reduced concentration $\phi(z) < \phi$ in the fluidized bands allows flow for σ (very) slightly below the average σ_y . Thus the determined σ_y for large ϕ may be slightly underestimated, preventing exact calculation of $\dot{\gamma}(r)$ for large ϕ where $\dot{\gamma}_c$ is large. Therefore, we have only analyzed the slip to yield transition for $[v(z_g) - v(z = 0)]/z_g > \dot{\gamma}_c$, i.e. where the induced bulk flow is essentially linear.

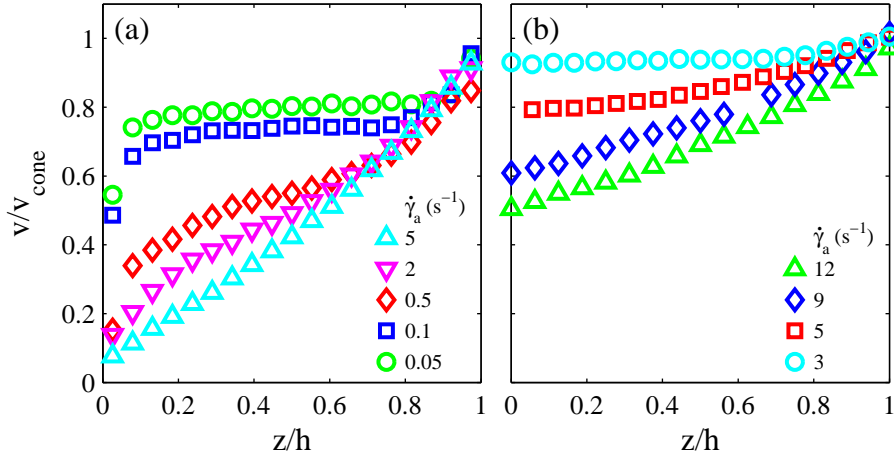


FIG. 16. (a) Velocity profiles for $\phi = 0.62$, $r = 5$ mm and both surfaces coated, for various $\dot{\gamma}_a$. (b) Same as (a) but for coated cone, smooth plate and $r = 5.5$ mm.

VIII. SLIP BELOW THE GLASS TRANSITION

In our earlier work [Ballesta *et al.* (2008)], we reported that for concentrations well below the glass transition, $\phi < \phi_g$, the flow curves and velocity profiles showed no indication of slip or shear-banding independent on the surface roughness. Figure 17 illustrates this for $\phi = 0.52$ where the flow curves for coated and smooth surfaces are essentially identical and the flow profiles (Fig.17 (b)) are very close to linear for all $\dot{\gamma}_a$. However, recent velocimetry data for suspensions closer to the glass transition clearly reveal slip at the lowest applied shear rate, although the effect is not detectable in the rheology of these samples.

Figure 18 shows the flow curve and velocity profiles for a $\phi = 0.535$ suspension with coated cone and smooth glass surface. In the flow curve, inset to Fig. 18(a), the low $\dot{\gamma}_a$ Newtonian behavior could not be resolved; only the shear thinning behavior could be detected. However, the velocity profiles in Fig. 18(a) clearly show slip, but with a finite bulk shear rate $\dot{\gamma} > 0$ (no plug flow), similar to what is observed in glassy samples for $\sigma > \sigma_y$. We extracted the dependence of $\dot{\gamma}$ on v_s for various gap sizes. The results in Fig. 18(b) show that $\dot{\gamma} = C v_s^2$. This is consistent with the model presented earlier, but taking into account the fact that in the concentrated liquid regime (here $\phi = 0.535$) the yield stress is absent. Using $\sigma_s = 0$, we obtain $\sigma \simeq \beta v_s$ and $\sigma = \alpha \dot{\gamma}^{0.5}$ giving $C = (\beta/\alpha)^2$. From the imaging data in Fig. 18(b) we find $C = 0.13 \cdot 10^{12}$ s/m² at this ϕ . To compare this with the rheology, a fit of the flow curve gives $\alpha = 0.177$ Pa.s^{0.5}, while β follows from extrapolation of the relation $\beta =$

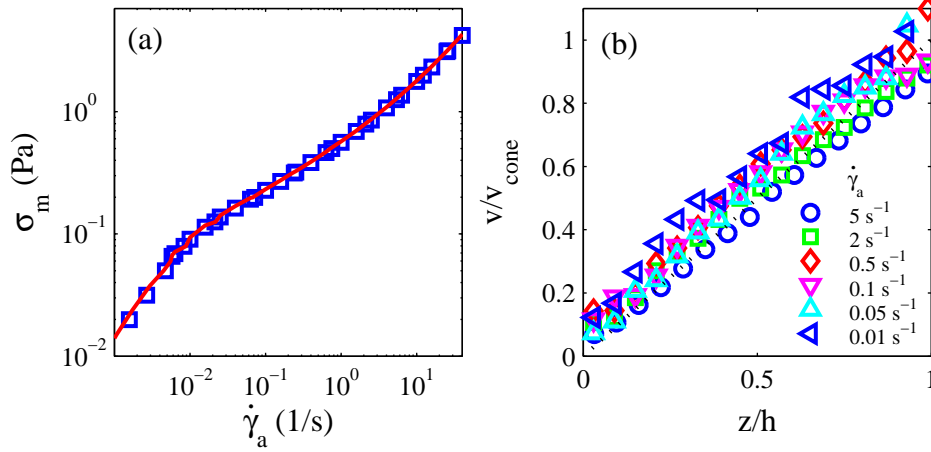


FIG. 17. (a) Flow curve for an RI-matched suspension with $a = 138$ nm, $\phi = 0.52$, with smooth (\square) and rough walls (full line). (b) $v(z)$ for smooth walls at $r = 5.5$ mm and for various $\dot{\gamma}_a$.

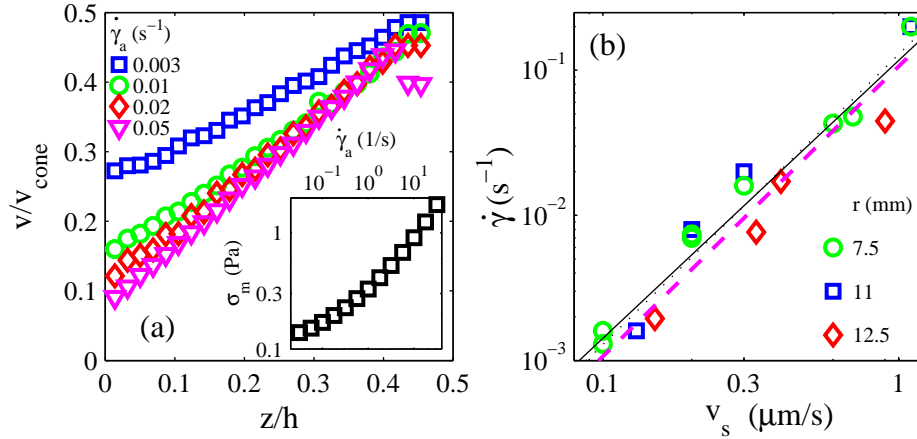


FIG. 18. (a) Normalized flow profiles at $r = 12.5$ mm for $\phi = 0.535$ at various $\dot{\gamma}_a$ using a smooth cone and smooth glass. Inset: measured flow curve. (b) Local shear rate $\dot{\gamma}$ versus slip velocity v_s at various r . Full line: fit to a power law $\dot{\gamma} \propto v_s^\nu$ with $\nu = 1.92 \pm 0.3$. Dotted line: $\dot{\gamma} = C v_s^2$ with $C = 0.13 \cdot 10^{12}$ s/m². Magenta discontinued line: $\dot{\gamma} = C v_s^2$ with $C = (\beta/\alpha)^2$ (see text).

$0.9\eta_s a^{-1}(\phi_{rcp} - \phi)^{-1}$ in the glassy state. This yields $\beta \simeq 5.8 \cdot 10^4$ Pa.s/m at this ϕ , giving $(\beta/\alpha)^2 = 0.11 \cdot 10^{12}$ s/m², in very reasonable agreement with the data. The model can thus also describe residual slip of liquids, assuming $\sigma_{s,y} = 0$.

We can compare the slip behavior of glasses and liquids further as follows. The rheology of liquid-like suspensions at low $\dot{\gamma}$ is characterized by a Newtonian flow ($\sigma = \eta_0 \dot{\gamma}$

with $\eta_0 = \eta_0(\phi)$ the zero shear viscosity), which evolves towards nonlinear shear thinning behavior at higher shear rates ($\sigma \propto \dot{\gamma}^n$). As a result of the low shear rate Newtonian behavior, any applied stress results in shear at all r 's for any such small $\dot{\gamma}_a$. At small $\dot{\gamma}$, the reduced apparent viscosity is $\eta_m = \eta_0/(1 + \eta_0/\beta h)$ (in plate-plate approximation⁶). A rough estimate of the difference between slip and no slip measurements can be obtained by using the phenomenological form for the divergence $\eta_0(\phi)$ on approaching the glass transition (e.g. [Meeker *et al.* (1997)]): $\eta_0 = \eta_s(1 - \phi\phi_g^{-1})^{-2}$ and the earlier mentioned extrapolation of $\beta = 0.9\eta_s a^{-1}(\phi_{rcp} - \phi)^{-1}$ to $\phi < \phi_g$. For $\phi = 0.52$, $a = 138$ nm and $h = 50$ μ m this leads to $\eta_m = 0.9588\eta_0$. A $\sim 4\%$ difference is roughly within the experimental uncertainty, which explains why we did not note slip at low ϕ in [Ballesta *et al.* (2008)]. However, as ϕ approaches ϕ_g , η_0 diverges while η_m tends towards βh and slip becomes apparent. For intermediate and large $\dot{\gamma}$, where the rheology can be approximated by $\sigma \propto \dot{\gamma}^n$ with $n \simeq 0.5$ (as stated above, and in agreement with a semi-empirical expression in Krieger (1959)), a calculation of the flow curves with and without slip shows that in all cases the relative difference between η_m and η increases with ϕ and decreases as $\dot{\gamma}_a$ increases, similarly to the glassy state. Since in the low-shear Newtonian regime the difference is already small (except very close to ϕ_g), the presence of slip is even more difficult to detect in the nonlinear rheology of liquids at larger rate. However, for $\phi > \phi_g$ the presence of a yield stress and plug flow leads to a stress difference $\sim \sigma_y$ regardless of the geometry, which explains why slip is easily detected in the rheology of HS glasses both for low and intermediate shear rates.

IX. DISCUSSION AND CONCLUSIONS

The rheology and velocimetry results and the modeling we presented clearly show that local particle-wall interactions, the character of the boundaries, the geometry and ϕ dependent nonlinear bulk rheology strongly affect the measured rheology of concentrated HS suspensions. In general for yield stress fluids, if a flow curve exhibits a ‘kink’ and a stress drop at low $\dot{\gamma}_a$ (with a power law $\dot{\gamma}_a^m$) that is absent when rough surfaces are used, one can conclude that (i) the sample slips at one or both surfaces and (ii) locally the transmitted stress is proportional to v_s^m , independent of the geometry. The detailed phenomenological

⁶ In cone-plate, setting $h = r \tan(\theta)$ and integrating as in Eq. 9, the refined expression for the apparent viscosity of a Newtonian liquid with slip is $\eta_m/\eta_0 = 1 - 2x_c[1 - x_c \ln(1 + x_c^{-1})]$ with $x_c = \eta_0/(\beta\theta r_c)$.

model we presented shows that, from a well characterized slip law $\sigma(v_s)$ and bulk rheology, the overall flow curve and local flow profiles can be accurately predicted (if more complex behavior such as shearbanding and possible non-stationary behavior can be ignored).

For our HS glasses with smooth non-stick walls, a velocity independent, but ϕ -dependent, lubrication layer forms, leading to $m = 1$, but vdW attractions, in non-RI-matched suspensions, easily suppress slip, leading to a slip stress $\sigma_s \geq \sigma_y$. Standard (non-imaging) rheology experiments for HSs are therefore unlikely to be affected by slip. Yet, with many recent studies of nonlinear colloidal flow focusing on microscopic properties [Cohen *et al.* (2006); Besseling *et al.* (2007)] via microscopy on RI matched suspensions, slip is an important ingredient, and we have shown here that the slip response can be related semi-quantitatively to a bulk property of the suspension (osmotic pressure). For other yield stress fluids, in particular jammed emulsions, the slip behavior may follow a different powerlaw, i.e. $m \simeq 0.5$ has been observed in [Meeker *et al.* (2004b); Seth *et al.* (2008)] due to elasto-hydrodynamic lubrication for non-repulsive smooth walls. *With* repulsion, $m \simeq 1$ is recovered, implying that our model of the slip-yield transition may carry over to emulsions. Further, emulsions with $\phi_g \lesssim \phi \lesssim \phi_{rcp}$ exhibit HS like (Brownian) glassy behavior [Gang *et al.* (1999)], for which we thus expect similar Bingham slip behavior as for the HSs.

In non-Brownian suspensions [Jana *et al.* (1995); Soltani and Yilmazer (2008); Kalyon (2005)], slip is also characterized by $m \simeq 1$, i.e. $\sigma \propto v_s$, i.e. a lubrication layer with a thickness independent of v_s [Kalyon (2005); Yilmazer and Kalyon (1989)]. Here, contrary to colloids, no slip stress is observed, as expected from the (near) absence of osmotic or wall-interaction effects. However, the detailed mechanism for slip in non-Brownian systems is still unclear as shown by the different phenomenological relations found: $\delta/a \simeq 0.125$ for concentrated but Newtonian suspensions ([Jana *et al.* (1995)], ϕ -independent), $\delta/a \simeq 0.06 - 0.15$ (for pastes of polydisperse spheres [Soltani and Yilmazer (2008)]), and $\delta/a \simeq 2/[1 - (\phi/\phi_{rcp})]$ ([Kalyon (2005)], for systems including polydisperse and non-spherical particles). Interestingly, the latter is similar to our Eq. 17 for the slip of colloidal glasses, but lacks a theoretical basis for non-Brownian systems. Moreover, in the latter two cases, slip was measured for non-uniform stress, such that shear induced migration may affect the interpretation.

We can also compare the results with those for (depletion) flocculated colloidal gels in [Buscall *et al.* (1993)]. There, a linear slip response has also been observed, with δ decreasing from $\sim 1\mu\text{m}$ to $\sim 10\text{ nm}$ from $\phi \sim 0.2$ to $\phi \sim 0.55$, without significant dependence

on particle size or colloid attraction strength. Here the nature of the slip layer is likely determined by the ϕ dependent aggregate lengthscale and structure, rather than the particle size. It is worth noting again that in these systems, even significant colloid-wall attraction is generally unable to suppress slip; unless the wall roughness is very large, the boundary typically acts as a weak ‘fracture’ plane and a slip response is induced. Insight in the nature of this behavior and a theoretical understanding are still lacking.

In conclusion, we have shown the existence of Bingham-type slip response in colloidal HS glasses near smooth non-stick walls. A phenomenological model quantitatively accounts for the global rheology and local flow profiles. Slip in HS glasses is effectively caused by Brownian motion, creating a lubrication layer and slip response governed by the suspensions osmotic pressure, evidenced by the particle size dependence and divergence for $\phi \rightarrow \phi_{rcp}$ of the slip stress and slip viscosity. For HSs, slip is suppressed by colloidal scale wall roughness or sufficient vdW wall attraction. Slip can also occur in concentrated liquid-like suspensions, but is *partial* ($\dot{\gamma}_a > \dot{\gamma} \neq 0$) due to absence of a yield stress. This is also described within the phenomenological model, but has only limited effect on the bulk rheology. Our study of HSs and the study of [Meeker *et al.* (2004b); Seth *et al.* (2008)] for emulsions, together with future similar studies for other yield stress fluids, should provide improved predictability of yield stress fluid flows in industrial processing and applications.

1. Acknowledgements

We thank K.N. Pham, J. Arlt and N. Pham for advice and help with the experiments, A.B. Schofield for particle synthesis and sizing and M.E. Cates, A. Morozov and D. Marenduzzo for useful discussions. R.B. and W.P. acknowledge funding through EP/D067650 and EP/D071070/1. L.I. was funded by the EU network MRTN-CT-2003-504712. G. P. and P. B. acknowledge EU funding from ToK “Cosines” (MTCDCCT-2005-029944), NMP Small “Nanodirect” (CPFP7- 213948-2) and NoE “SoftComp”.

Appendix A: Local and global rheology in cone-plate geometry

1. Slip at one surface

This is the case in most of our experiments. Slip occurs at the bottom plate and we set $\sigma_1 = \infty$ (i.e. $v_1 = 0$) and $\sigma_2 < \sigma_y$. In a cone-plate, the relative stress inhomogeneity over the gap is $\simeq \theta^2$. This is negligible in our case and we take σ uniform at a given r . Using Eqs. (2,4) with $h = r \tan(\theta)$ we have:

$$\sigma(r) = \beta r \tan(\theta) [\dot{\gamma}_a - \dot{\gamma}(r)] + \sigma_2. \quad (\text{A1})$$

The stress measured with the rheometer follows from Eq. (9) in Sec. IV. We define the critical applied shear rate $\dot{\gamma}_{a,c} = (\sigma_y - \sigma_2) / \beta r_c \tan(\theta)$ such that for $\dot{\gamma}_a < \dot{\gamma}_{a,c}$, the bulk shear rate vanishes over the entire geometry (regime I). The measured stress is then given by Eq. (10) in Sec. IV B. When $\dot{\gamma}_a > \dot{\gamma}_{a,c}$ (regime II), we define $r_y = (\sigma_y - \sigma_2) / (\beta \tan(\theta) \dot{\gamma}_a)$ such that $\dot{\gamma} = 0$ for $r \leq r_y$ and $\dot{\gamma} > 0$ for $r > r_y$. The integral in Eq. (10) consists of two parts: solid body rotation for $r < r_y$ and slip and shear for $r > r_y$. Using Eq. (5) and Eq. (6) with $h = r \tan(\theta)$ and Eq. (A1) gives the following result:

$$\begin{aligned} \sigma_m^{\text{II}} = & \sigma_y - \frac{\Delta\sigma^3}{3\sigma_E^2} - \frac{\sigma_R^2}{\sigma_E} \\ & + \frac{\sigma_R^2}{\sigma_E} \left(\frac{3\Delta\sigma}{4\sigma_E} + \left(\frac{1}{2} - \frac{\Delta\sigma}{4\sigma_E} \right) \sqrt{1 + \frac{4\sigma_E^2}{\sigma_R^2} \left(1 - \frac{\Delta\sigma}{\sigma_E} \right)} \right) \\ & + \left(\frac{\sigma_R^3}{4\sigma_E^2} - \frac{\Delta\sigma^2 \sigma_R}{4\sigma_E^2} \right) \log \left(\frac{2\frac{\sigma_E}{\Delta\sigma} - 1 + \sqrt{\frac{\sigma_R^2}{\Delta\sigma^2} + \frac{4\sigma_E}{\Delta\sigma} \left(\frac{\sigma_E}{\Delta\sigma} - 1 \right)}}{1 + \frac{\sigma_R}{\Delta\sigma}} \right), \end{aligned} \quad (\text{A2})$$

with $\sigma_E = \beta \tan(\theta) r_c \dot{\gamma}_a$, $\sigma_R = \alpha \sqrt{\dot{\gamma}_a}$, and $\Delta\sigma = \sigma_y - \sigma_2$.

We have assumed that in regime II shear occurs only in the z direction, *i.e.* $\partial_r v = 0$. But because the (partial) slip velocity depends on r , in general $\partial_r v \neq 0$ during shear flow. This radial velocity gradient can be calculated from $v = \dot{\gamma} z$, where $\dot{\gamma}$ is given by Eq. (5) with $h = r \tan(\theta)$, with the result:

$$\partial_r v = z \partial_r \dot{\gamma} = \frac{z}{r} \left(\frac{\Delta\sigma}{h\beta} - 2\dot{\gamma}_0 + \frac{2\dot{\gamma}_0 + \left(2\dot{\gamma}_a - \frac{3\Delta\sigma}{h\beta} \right)}{\sqrt{1 + \frac{2}{\dot{\gamma}_0} \left(\dot{\gamma}_a - \frac{\Delta\sigma}{h\beta} \right)}} \right). \quad (\text{A3})$$

Hence, $\partial_r v$ tends to 0 for $r \rightarrow \infty$ and $r \rightarrow r_y$. However, approaching the boundary of the region with solid body, $r \rightarrow r_y$, the relative contribution $(\partial_r v) / \dot{\gamma}$ grows as:

$$\partial_r v / \dot{\gamma} \simeq 2z / (r - r_y) < 2r \tan(\theta) / (r - r_y). \quad (\text{A4})$$

The shear rate in the vorticity direction may thus be important for $r \simeq r_y$, but is negligible for $(r/r_y) - 1 \gg 2 \tan(\theta)$. For our case ($\theta = 1^\circ$), one can neglect $\partial_r v$ in practice, as confirmed by the agreement with the experiments, e.g. in Fig. 6.

2. Slip at both surfaces

We now also allow slip at the cone with $\sigma_2 \leq \sigma_1 < \sigma_y$. We first discuss solid body rotation in regime I_b, *i.e.* $\sigma_1 < \sigma < \sigma_y$. The suspensions angular velocity ω_{bulk} in this regime is determined as follows. The slip velocities at the top and bottom plates are given by $v_1 = (\omega - \omega_{\text{bulk}})r$ and $v_2 = \omega_{\text{bulk}}r$, respectively, with $\omega = \dot{\gamma}_a \tan(\theta)$. Since the total, integrated stress σ_m at the top ($\sigma_{\text{top}} = \sigma_1 + 2\beta(\omega - \omega_{\text{bulk}})r_c/3$) and bottom ($\sigma_{\text{bottom}} = \sigma_2 + 2\beta\omega_{\text{bulk}}r_c/3$) surfaces are equal, the solid body rotation velocity in regime I_b is:

$$v_{\text{bulk}} = r\dot{\gamma}_a \tan(\theta)/2 + 3(r/r_c)(\sigma_1 - \sigma_2)/4\beta. \quad (\text{A5})$$

As a result, for slip at both surfaces, the local stress $\sigma(r)$ differs between the cone and the plate, by an amount $\Delta\sigma(r) = (\sigma_1 - \sigma_2) \left(1 - \frac{3r}{2r_c}\right)$. The rate $\dot{\gamma}_a^*$ where the transition from slip at the plate (I_a) to slip at the plate and cone (I_b) occurs, is determined by equating the measured stress due to slip at the plate and that for slip at both surfaces, Eqs. (10,11):

$$\dot{\gamma}_a^* = 3(\sigma_1 - \sigma_2)/2\beta r_c \tan(\theta). \quad (\text{A6})$$

When $\dot{\gamma}_a$ increases and regime II is approached, the above calculation shows that shear will first occur at the edge of the bottom plate for $\dot{\gamma}_{a,e} = \frac{4\sigma_y - 3\sigma_1 - \sigma_2}{2\beta r_c \tan(\theta)}$. The local stress difference between the top and bottom plate makes a complete description of shear propagation into the cell very difficult. However since $\sigma_1 - \sigma_2$ is often small compared to σ_y some approximations can be made. We assume that shear occurs at the same position r_y for the cone and the plate and that in the sheared region of the sample ($r > r_y$) the stress $\sigma(z)$ is uniform. For infinite parallel plates we already found that the flow with slip at both surfaces is described in the same way as slip at one surface by replacing $\beta \rightarrow \beta/2$ and $\sigma_2 \rightarrow (\sigma_1 + \sigma_2)/2$, see Eqs. (6,7). The same change of variables applied to the cone-plate leads to $r_y = (2\sigma_y - \sigma_1 - \sigma_2)/\beta\omega$ and a transition from regime I_b to II at $\dot{\gamma}_{a,c} = \frac{2\sigma_y - \sigma_1 - \sigma_2}{\beta r_c \tan(\theta)}$, which, with the approximation $\sigma_1 - \sigma_2 \ll \sigma_y$, is equivalent to $\dot{\gamma}_{a,e}$ above. We then again have shear and slip for $r > r_y$ and solid body rotation for $r < r_y$. The velocity for $r < r_y$ follows, as before, from the balance

between total stress on the bottom plate and cone:

$$v_{r < r_y} = \frac{r\dot{\gamma}_a \tan(\theta)}{2} \left(1 + \frac{3}{2} \frac{\sigma_1 - \sigma_2}{2\sigma_y - \sigma_1 - \sigma_2} \right). \quad (\text{A7})$$

For $\dot{\gamma}_a \geq \dot{\gamma}_{a,c}$, the measured stress is still given by eq. (A2) with the following changes: $\beta \rightarrow \beta/2$ and $\sigma_2 \rightarrow (\sigma_1 + \sigma_2)/2$.

3. Slip length

The relation between bulk and applied shear rate in regime II can also be expressed via a slip length. For slip at the bottom plate only, we have:

$$l_s = v_s/\dot{\gamma} = h(\dot{\gamma}_a - \dot{\gamma})/\dot{\gamma} \quad (\text{A8})$$

with v_s the slip velocity, h the gap and $\dot{\gamma}$ and $\dot{\gamma}_a$ the local and applied shear rate, respectively. The full dependence $l_s(\dot{\gamma}_a)$ follows directly from the relation $\dot{\gamma}(\dot{\gamma}_a)$, Eq. (5) and Eq. (6) in Sect. IV. For large shear rate, Taylor expansion of Eq. (5) in $\dot{\gamma}_a^{-1/2}$ results in:

$$l_s = h\sqrt{\frac{2\dot{\gamma}_0}{\dot{\gamma}_a}} + O(\dot{\gamma}_a^{-1}). \quad (\text{A9})$$

Figure 19 shows both the exact form for l_s from Eqs. (A8,5) and the high shear approximation, showing the divergence of l_s for $\dot{\gamma}_a \downarrow \dot{\gamma}_y$ and the asymptotic decrease $l_s \sim 1/\sqrt{\dot{\gamma}_a}$.

Appendix B: van der Waals interactions

The van der Waals interactions between two particles and between a particle and a wall were calculated according to [Gregory (1981); Hunter (2001)]. For a particle of radius a separated by a distance δ from the wall we have:

$$V_{pw} = -\frac{A_{132}a}{6\delta} \left(1 + \frac{\delta}{2a + \delta} + \frac{\delta}{a} \ln \left(\frac{\delta}{2a + \delta} \right) \right), \quad (\text{B1})$$

while the interaction between two colloids separated by a distance 2δ is:

$$V_{pp} = -\frac{A_{131}a}{24\delta} \left(\frac{2a}{2a + \delta} + \frac{2a\delta}{(a + \delta)^2} + \frac{4\delta}{a} \ln \left(\delta \frac{2a + \delta}{(a + \delta)^2} \right) \right). \quad (\text{B2})$$

For the interaction between the glass plate and particles, the Hamaker constant A_{132} , where the indexes $i = 1, 2, 3$ refer to PMMA, glass, and solvent, respectively (table II), is

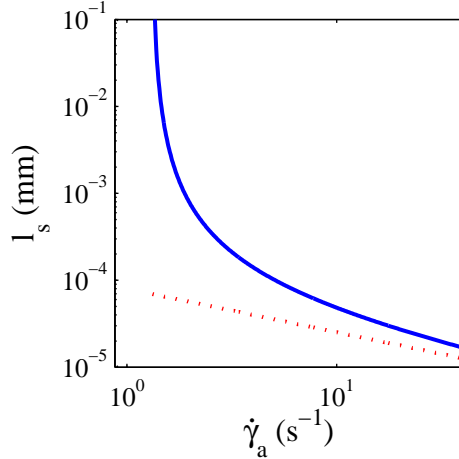


FIG. 19. Slip length l_s versus applied rate for $h = 50 \mu\text{m}$, $\alpha = 10 \text{ Pa}\cdot\text{s}^{1/2}$, $\beta = 1.25 \cdot 10^5 \text{ Pa}\cdot\text{s}\cdot\text{m}^{-1}$, $\sigma_y = 10.6 \text{ Pa}$ and $\sigma_s = 2.39 \text{ Pa}$. Full line is the exact form using Eq. (A8), Eq. (5) and Eq. (6) in Sect. IV, dotted line represents Eq. A9.

approximately [Lee and Komarneni (2005)]:

$$A_{132} = \frac{3k_B T}{4} \prod_{i=1}^2 \left(\frac{\epsilon_i - \epsilon_3}{\epsilon_i + \epsilon_3} \right) + \frac{3h\nu_e}{8\sqrt{2}} \frac{1}{\sum_{i=1}^2 \sqrt{n_i^2 + n_3^2}} \prod_{i=1}^2 \left(\frac{n_i^2 - n_3^2}{\sqrt{n_i^2 + n_3^2}} \right), \quad (\text{B3})$$

while the Hamaker constant between the steel cone (denoted by subscript 2) and the particles (1) through solvent (3) is estimated using the approach of [Lipkin *et al.* (1997)]:

$$A_{132} = \frac{3k_B T}{4} \frac{\epsilon_1 - \epsilon_3}{\epsilon_1 + \epsilon_3} + 3h\nu_e n_1 (n_1 - n_3) \left(\frac{1}{2n_1} - \frac{1}{\sqrt{2(n_1^2 + 2 + 2\sqrt{2})}} \right). \quad (\text{B4})$$

Here ϵ_i is the dielectric permittivity, n_i the respective indexes of refraction, h the Planck constant, and ν_e a characteristic frequency which for simplicity is equated with the lowest energy adsorption peak of PMMA in the ultraviolet $\nu_e = 0.3 \times 10^{16} \text{ Hz}$ (Hough and White (1980)).

REFERENCES

Aral, B.K. and D.M. Kalyon, “Effects of temperature and surface roughness on time-dependent development of wall slip in steady torsional flow of concentrated suspensions”, *J. Rheol.* **38**, 957–972 (1994).

- Ballesta, P., R. Besseling, L. Isa, G. Petekidis, and W. C. K. Poon, “Slip and Flow of Hard-Sphere Colloidal Glasses”, *Phys. Rev. Lett.* **101**, 258301 (2008).
- Barnes, H. A., “A review of the slip (wall depletion) of polymer solutions, emulsions and particle suspensions in viscometers: its cause, character, and cure”, *J. Non-Newtonian Fluid Mech.* **56**, 221–251 (1995).
- Barrett K.E.J. (Ed.), “Dispersion Polymerization in Organic Media,” Wiley-Blackwell (1974).
- Barrat, J. L. and L. Bocquet, “Large Slip Effect at a Non wetting Fluid-Solid Interface”, *Phys. Rev. Lett.* **82**, 4671–4674 (1999).
- Bécu, L., D. Anache, S. Manneville, and A. Colin, “Evidence for three-dimensional unstable flows in shear-banding wormlike micelles”, *Phys. Rev. E* **76**, 011503 (2007).
- Bécu, Lydiane and Manneville, Sébastien and Colin, Annie , “Spatiotemporal Dynamics of Wormlike Micelles under Shear”, *Phys. Rev. Lett.* **93**, 018301 (2004).
- Bertola, V., F. Bertrand, H. Tabuteau, D. Bonn, and P. Coussot, “ Wall slip and yielding in pasty materials”, *J. Rheol.* **47**, 1211 (2003).
- Besseling, R., E.R. Weeks, A.B. Schofield and W. C. K. Poon, “Three-dimensional imaging of colloidal glasses under steady shear”, *Phys. Rev. Lett.* **99**, 028301 (2007).
- Besseling, R., L. Isa, E. R. Weeks, and W. C. K. Poon, “Quantitative imaging of colloidal flows”, *Adv. Coll. Int. Sci.* **146**, 1–17 (2009).
- Besseling, R., L. Isa, P. Ballesta, G. Petekidis, M. E. Cates, and W. C. K. Poon, “Shear banding and flow-concentration coupling in colloidal glasses”, *Phys. Rev. Lett.* **105**, 268301 (2010).
- Bocquet, L. and J.-L. Barrat, “Flow boundary conditions from nano- to micro-scales”, *Soft Matter* **12**, 685–693 (2007).
- Bocquet, L. and A. Colin, and A. Adjari “Kinetic Theory of Plastic Flow in Soft Glassy Materials”, *Phys. Rev. Lett.* **103**, 036001 (2009).
- Brady, J. F. “The rheological behavior of concentrated colloidal dispersions”, *J. Chem. Phys.* **99**, 567—581 (1993).
- Brady, J.F. and M.A. Vicic, “Normal stresses in colloidal dispersions”, *J. Rheol.* **39**, 545–566 (1995).
- Brady, J. F. “Model hard-sphere dispersion: statistical mechanical theory, simulations and experiments”, *Curr. Op. Coll. Int. Sci.* **1**, 472–480 (1996).

- Brochardt, F. and P. G. de Gennes, “Shear-Dependent Slippage at a Polymer/Solid Interface”, *Langmuir* **8**, 3033–3037 (1992).
- Bryant, G., S. R. Williams, L. Qian, I. K. Snook, E. Perez, and F. Pincet, “How hard is a colloidal ‘hard-sphere’ interaction?”, *Phys. Rev. E* **66**, 060501 (2002).
- Buscall, R., J. I. McGowan, and A. J. Morton-Jones, “The rheology of concentrated dispersions of weakly attracting colloidal particles with and without wall slip”, *J. Rheol.* **37**, 621–641 (1993).
- Buscall, J., “Wall slip in dispersion rheometry”, *J. Rheol.* **54**, 1177–1183 (2010).
- Cohen, I., B. Davidovitch, A. B. Schofield, M. P. Brenner, and D. A. Weitz, “Slip, Yield, and Bands in Colloidal Crystals under Oscillatory Shear”, *Phys. Rev Lett.* **97**, 215502 (2006).
- Coussot, P., J. S. Raynaud, F. Bertrand, P. Moucheron, J. P. Guilbaud, H. T. Huynh, S. Jarny, and D. Lesueur, “Coexistence of Liquid and Solid Phases in Flowing Soft-Glassy Materials”, *Phys. Rev. Lett.* **88**, 218301 (2002).
- Denkov, N. D., S. Tcholakova, K. Golemanov, V. Subramanian, and A. Lips, “Wall slip and viscous dissipation in sheared foams: Effect of surface mobility”, *Coll. Surf. A* **263**, 129–145 (2005).
- Dullens, R. P. A. and W. K. Kegel, “Reentrant Surface Melting of Colloidal Hard Spheres”, *Phys. Rev. Lett.* **92**, 195702, 2004.
- Derks, D., H. Wisman, A. van Blaaderen, and A. Imhof, “Confocal microscopy of colloidal dispersions in shear flow using a counter-rotating cone–plate shear cell”, *J. Phys.: Condens. Matter* **16**, S3917–S3927 (2004).
- Proceedings Symposium IEEE/LEOS Benelux Chapter, 2007, Brussels A Quasi-Optical Free-Space Method for Dielectric Constant Characterization of Polymer Materials in mm-wave Band A.Elhawil, L. Zhang , J. Stiens, C. De Tandt, N. A. Gotzen, G. V. Assche, R. Vounckx
- Hermes, M, and M. Dijkstra, “Jamming of polydisperse hard spheres: The effect of kinetic arrest”, *Europhys. Lett.* **89**, 38005 (2010).
- Gang, H., A. H. Krall, H. Z. Cummins, and D. A. Weitz, “Emulsion glasses: A dynamic light-scattering study”, *Phys. Rev. E* **59**, 715–721 (1999).
- Gibaud, T., C. Barentin, and S. Manneville, “Influence of Boundary Conditions on Yielding in a Soft Glassy Material”, *Phys. Rev. Lett.* **101**, 258302 (2008).

- Goldman, A.J., R. G. Cox, and H. Brenner, “Slow viscous motion of a sphere parallel to a plane wall. 1 Motion through a quiescent fluid”, *Chem. Eng. Sci.* **22**, 637–651 (1967).
- J.P. Gong and Y. Osada, “Soft and Wet Materials: From Hydrogels to Biotissues”, *Adv. Polym. Sci.* **236** 203–246, Ed. M. Cloitre, Springer-Verlag Berlin Heidelberg (2010).
- Gregory, J., ‘Approximate Expressions for Retarded van der Waals Interaction’, *J. Colloid Interface Sci.* **83**, 138–145 (1981).
- Hartman Kok, P. J. A., S. G. Kazarian, B. J. Briscoe, and C. J. Lawrence, “Effects of particle size on near-wall depletion in mono-dispersed colloidal suspensions”, *J. Col. Int. Sci* **280**, 511–517 (2004).
- Hatzikiriakos, S. G. and J. M. Dealy, “Wall slip of molten high density polyethylene I. Sliding plate rheometer studies”, *J. Rheol.* **35**, 497–523 (1991).
- Hatzikiriakos, S. G. and J. M. Dealy, “Wall slip of molten high density polyethylene II. Capillary rheometer studies”, *J. Rheol.* **36**, 703–741 (1992).
- Henderson, J.R. and F. van Swol, “On the interface between a fluid and a planar wall. Theory and simulations of a hard sphere fluid at a hard wall”, *Mol. Phys.* **51**, 991–1010 (1984).
- Hough, D. B. and L. R. White, “The calculation of Hamaker constant from Lifshitz theory with application to wetting phenomena”, *Adv. Colloid. Interface Sci.* **14**, 3–41 (1980).
- Hunter R.J., *Foundations of Colloid Science*, (Oxford University Press, New York, 2001).
- Isa, L., R. Besseling, and W. C. K. Poon, “Shear Zones and Wall Slip in the Capillary Flow of Concentrated Colloidal Suspensions”, *Phys. Rev. Lett.* **98**, 198305 (2007).
- Jana, S. C., B. Kapoor, and A. Acrivos, “Apparent wall slip velocity coefficients in concentrated suspensions of noncolloidal particles”, *J. Rheol.* **39**, 1123–1132 (1995).
- Kalyon, D. M., “Apparent slip and viscoplasticity of concentrated suspensions”, *J. Rheol.* **49**, 621–640 (2005).
- Katgert, G., M. E. M3bius, and M. van Hecke, “Rate Dependence and Role of Disorder in Linearly Sheared Two-Dimensional Foams”, *Phys. Rev. Lett.* **101**, 058301 (2008).
- Koumakis, N., A. Pamvouxoglou, A. Poulos, and G. Petekidis, “Direct comparison of the rheology of hard and soft particle glasses”, *Soft Matter*, in press (2012).
- Krieger, I. M. and T. J. Dougherty, “A Mechanism for Non-Newtonian Flow in Suspensions of Rigid Spheres”, *Trans. Soc. Rheol.* **3**, 152 (1959)
- Larson, R. G., *The Structure and Rheology of Complex Fluids* (Oxford University Press,

- New York, 1999);
- Lee, B. and S Komarneni , *Chemical Processing of Ceramics, Second Edition* (CRC Press, 2005);
- Léger, L., H. Hervet, G. Massey, and E. Durliat, “Wall slip in polymer melts”, *J. Phys.: Condens. Matter* **9** 7719–7740 (1997).
- Lettinga, M. P., and S. Manneville, “Competition between Shear Banding and Wall Slip in Wormlike Micelles”, *Phys. Rev. Lett.* **103** 248302 (2009).
- Lipkin, D. M., J. N. Israelachvili, and D. R. Clarke, “Estimating the metal-ceramic van der Waals adhesion energy”, *Phil. Mag. A* **76**(4), 715–728 (1997).
- Manneville, S., L. Bécu, and A. Colin, “High-frequency ultrasonic speckle velocimetry in sheared complex fluids”, *Eur. Phys. J. Appl. Phys.* **28**, 361–373 (2004).
- Meeker, S. P., W. C. K. Poon, and P. N. Pusey, “Concentration dependence of the low-shear viscosity of suspensions of hard-sphere colloids”, *Phys. Rev. E* **55**, 5718—5722 (1997)
- Meeker, S. P., R. T. Bonnecaze, and M. Cloitre, “Slip and Flow in Soft Particle Pastes”, *Phys. Rev. Lett.* **92**, 198302 (2004)
- Meeker, S. P., R. T. Bonnecaze, and M. Cloitre, “Slip and flow in pastes of soft particles: Direct observation and rheology”, *J. Rheol.* **48**, 1295–1320 (2004).
- Mhetar, V. and L. A. Archer, “Slip in Entangled Polymer Melts. 1. General Features”, *Macromolecules* **31**, 8607-8616 (1998).
- Michailidou, V., G. Petekidis, J. W. Swan, and J. F. Brady, “Dynamics of Concentrated Hard-Sphere Colloids Near a Wall”, *Phys. Rev. Lett.* **102**, 068302 (2009).
- Neto, C., D. R. Evans, E. Bonaccorso, H.-J. Butt, and V. S. J. Craig, “Boundary slip in Newtonian liquids: a review of experimental studies”, *Reports on Progress in Physics* **68**, 2859–2897 (2005).
- Persello, J., A. Magnin, J. Chang, J.-M. Piau, and B. Cabane, “Flow of colloidal aqueous silica dispersions”, *J. Rheol.* **38**, 1845–1870 (1994).
- Petekidis, G., D. Vlassopoulos, and P. N. Pusey, “Yielding and flow of sheared colloidal glasses”, *J. Phys. Cond. Mat.* **16**, S3955—S3963 (2004).
- Pham, K. N., G. Petekidis, D. Vlassopoulos, S. U. Egelhaaf, P. N. Pusey, and W. C. K. Poon, “Yielding of colloidal glasses”, *Europhys. Lett.* **75**, 624–630 (2006).
- Pham, K. N., G. Petekidis, D. Vlassopoulos, S. U. Egelhaaf, P. N. Pusey, and W. C. K. Poon, “Yielding behavior of repulsion- and attraction dominated colloidal glasses”, *J. Rheol.* **52**,

- 649–676 (2008).
- Phan, S.-E., W. B. Russel, Z. Cheng, J. Zhu, P. M. Chaikin, J.H. Dunsmuir, and R. H. Ottewill, “Phase transition, equation of state, and limiting shear viscosities of hard sphere dispersions”, *Phys. Rev. E* **54**, 6633–6645 (1996).
- Polverari, M. and T. G. M. van de Ven, “Effect of Flow on the Distribution of Colloidal Particles near Surfaces Studied by Evanescent Wave Light Scattering”, *Langmuir* **11**, 1870–1876 (1995).
- Poon, W. C. K., E. R. Weeks, and C. P. Royall, “On measuring colloidal volume fractions”, *Soft Matter* **8**, 21–30 (2012).
- Princen, H. M., “Rheology of foams and highly concentrated emulsions. II. Experimental study of the yield stress and wall effects for concentrated oil-in-water emulsions”, *J. Colloid Interface Sci.* **105**, 150–171 (1985).
- Pusey, P. N., and W. van Megen, “Phase behaviour of concentrated suspensions of nearly hard colloidal spheres”, *Nature* **320**, 340–342 (1986).
- Quemada, D., “Rheology of concentrated disperse systems and minimum energy dissipation principle. I. Viscosity-concentration relationship”, *Rheol. Acta* **16**, 82–94 (1977).
- Russel, W. B. and M. C. Grant, “Distinguishing between dynamic yielding and wall slip in a weakly flocculated colloidal dispersion”, *Colloids Surf. A* **161**, 271–282 (2000).
- Salmon, J.-B., S. Manneville, and A. Colin, “Shear banding in a lyotropic lamellar phase. I. Time-averaged velocity profiles”, *Phys. Rev. E* **68**, 051503 (2003).
- Salmon, J.-B., S. Manneville, A. Colin, and B. Pouligny, “An optical fiber based interferometer to measure velocity profiles in sheared complex fluids”, *Eur. Phys. J. Appl. Phys.* **22**, 143–154 (2003); “Towards local rheology of emulsions under Couette flow using Dynamic Light Scattering”, *Eur. Phys. J. E* **10**, 209–221 (2003).
- Schaertl W. and Sillescu H., “Brownian Dynamics of Polydisperse Colloidal Hard Spheres: Equilibrium Structures and Random Close Packings”, *J. Stat. Phys.* **77**, 1007–1025 (1994)
- Schmitt, V., C. M. Marques, and F. Lequeux, “Shear-induced phase separation of complex fluids: The role of flow-concentration coupling”, *Phys. Rev. E* **52**, 4009–4015 (1995).
- Segré, P. N., O. P. Behrend, and P. N. Pusey, “Short-time Brownian motion in colloidal suspensions: Experiment and simulation”, *Phys. Rev. E* **52**, 5070–5083 (1995).
- Seth, R., R. T. Bonnecaze, and M. Cloitre, “Influence of short-range forces on wall-slip in microgel pastes”, *J. Rheol.* **52**, 1241–1268 (2008).

- Sharma, P., S. Ghosh, and S. Bhattacharya, “Microrheology of a sticking transition”, *Nature Physics* **4**, 960–966 (2008).
- Soltani, F., and U. Yilmazer, “Slip velocity and slip layer thickness in flow of concentrated suspensions”, *J. Appl. Pol. Sci.* **70**, 515–522 (1998).
- Swan, J. “Colloids in confined geometries: hydrodynamics, simulation and rheology”, Thesis, California Institute of Technology Pasadena, California.
- Tokuyama, M. and Y. Terada, “How different is a hard-sphere fluid from a suspension of hard-sphere colloids near the glass transition”, *Physica A* **375**, 18–36 (2007).
- van Meegen, W., T. C. Mortensen, S. R. Williams, and J. Müller, “Measurements of the self-intermediate scattering function of suspensions of hard spherical particles near the glass transition”, *Phys. Rev. E* **58**, 6073–6085 (1998).
- Varadan, P., M. J. Solomon, “Direct visualization of flow-induced microstructure in dense colloidal gels by confocal laser scanning microscopy”, *J. Rheo.* **47**, 943–968 (2003).
- Walls, H. J., S. B. Caines, A. M. Sanchez, and S. A. Khan, “Yield stress and wall slip phenomena in colloidal silica gels”, *J. Rheo.* **47**, 847–868 (2003).
- Wassenius, H. and P.T. Callaghan, “NMR velocimetry studies of the steady-shear rheology of a concentrated hard-sphere colloidal system”, *Eur. Phys. J. E* **18**, 69–84 (2005).
- Westover, R. C., “The Significance of Slip in Polymer Melt Flow”, *Polym. Eng. Sci.* **6**, 83–89 (1966).
- Yilmazer, U. and D. M. Kalyon, “Slip Effects in Capillary and Parallel Disk Torsional Flows of Highly Filled Suspensions”, *J. Rheol.* **33**, 1197–1212 (1989).
- Yoshimura, A. and R. K. Prud’homme, “Wall Slip Corrections for Couette and Parallel Disk Viscometers” *J. Rheol.* **32**, 53–67 (1988).
- Zhu, Y., S. Granick, “Rate-Dependent Slip of Newtonian Liquid at Smooth Surfaces”, *Phys. Rev. Lett.* **87**, 096105 (2001); “Limits of the Hydrodynamic No-Slip Boundary Condition”, *Phys. Rev. Lett.* **88**, 106102 (2002).